PCCP

Accepted Manuscript

ROYAL SOCIETY OF CHEMISTRY

www.rsc.org/pccp

PCCP

ARTICLE

Effects of Drying Temperature and Ethanol Concentration on Bipolar Switching Characteristics of Natural Aloe Vera-Based Memory Devices

Received 04th August 2015,
Accepted 00th January 20xx

DOI: 10.1039/x0xx00000x

www.rsc.org/pccp

Zhe Xi Lim[a] and Kuan Yew Cheong[*a]

Extracted, formulated, and processed natural Aloe vera has been used as an active layer for memory application. The functional memory device is realized in a bottom-up structure of ITO/Aloe vera/Al, in which the Aloe vera is spin-coated after mixing with different concentrations of ethanol (0–80 wt%) and subsequently dried at different temperatures (50–120°C). From the current density–voltage measurements, a reproducible bipolar switching characteristic can only be exhibited by the device with pure Aloe vera dried at 50°C. It is proposed that charges are transported the Aloe vera layer via space-charge-limited conduction (SCLC) and clusters of interstitial space formed by the functional groups of acemannans and de-esterified pectins in the dried Aloe vera are contributing to the memory effect. The formation of charge traps in Aloe vera layer is dependent on the drying temperature. The drying temperature of a memory-switching Aloe vera layer can be extended to 120°C with the addition of ethanol in appropriate amounts. The concept of using natural Aloe vera as an active material for memory application has been proven, in which the read memory window, ON/OFF ratio, and retention time are approximately 5.0 V, 10^3, and >10^4 s.

Introduction

Rapid technological advancement has driven the world towards the verge of Internet of Things (IOTs),[1] where various electronic devices will be connected to a common network for information exchange. Unlike those in previous generations, future electronic devices that serve only a specific purpose will be produced with lower cost, higher volume, and shorter useful lifespan–the rise of disposable electronics.[2,3] The phenomenal growth of disposable electronics is often controversial, mainly because of the negative impacts that it does on the environment. The excessive exploitation of non-renewable resources such as inorganic minerals (Ga, Ti, and rare-earth elements) and organic materials (plastics and synthetic polymers derived from petroleum feedstock) for disposable electronics is not sustainable.[4,5] More importantly, there is a growing concern of massive pilling up of electronic waste (e-waste) in landfills that may take years to decompose.[2-6]

The urge to address the environmental issues is opening up opportunities for natural materials as a viable alternative for electronic applications. Natural materials offer not only a green and sustainable solution to the environmental issues, but also a compelling concept for electronics manufacturing. The innate biodegradability and biocompatibility render them with the capability to overcome the e-waste crisis.[6-9] Additionally, the use of natural materials could bring further cost reduction owing to their abundance and accessibility in the nature. Moreover, the absence of complicated chemical synthesis and purification steps in natural materials-based electronics could lead to a simpler manufacturing process that demands relatively less energy. Due to the unique properties and advantages of natural materials, there have been several reports addressing the initial use of natural materials for various electronic applications.[4,7-14]

Of these electronic applications, the use of natural materials for memory application is of particular interesting because the realization of IoTs will foresee the generation of an enormous amount of data, which ultimately have to be stored in memory devices for processing into interpretable formats. In general, a memory device is a basic electronic component that can store a digital data over a prolonged period of time.[15] Natural materials with reported memory-switching characteristics in a metal/natural material/metal structure include tobacco mosaic virus (TMV),[16] ferritin,[17] lysozyme (LYS),[18] silk fibroin,[19-21] sericin,[22] cellulose nanofiber paper (CNP),[23] chitosan,[24] DNA,[25] and chicken egg albumen[26] (Table 1). Using the same structure, the memory devices are termed differently, with bio-memristor and resistive random-access memory (ReRAM) among the most popular terminologies. Despite the fact that natural materials occur as a mixture of chemical composition in the nature, only a specific compound of the composition is held responsible for inducing memory switching. While some reports have incorporated the necessary purification steps, there are no

[a] Electronic Materials Research Group, School of Materials & Mineral Resources Engineering, Engineering Campus, Universiti Sains Malaysia, 14300 Nibong Tebal, Pulau Pinang, Malaysia. E-mail: srcheong@usm.my; Tel.: +604-599 5259; Fax: +604- 594 1011.

Table 1. Natural materials that have demonstrated memory switching effects in bottom-up structures of top electrode/natural materials/bottom electrode.

Year	Natural material	Device terminology	Substrate	Electrodes		Responsible compound	Purification	Ref.
				Top	Bottom			
2006	Tobacco mosaic virus (TMV)	Digital memory	Glass	Al	Al	TMV-Pt nanoparticle blend	X	16
2011	Ferritin	Nonvolatile memory	Si/SiO_2	Ag, W, Pt	Pt	PAH/ferritin nanoparticle layers	X	17
2012	Lysozyme (LYS)	Resistive switching memory	Si/SiO_2	Ag, Au, W, Pt	Pt	LYS/PSS, LYS/PSS/PAH/PSS, or LYS/PAA/PAH/PAA layers	X	18
2012	Silk fibroin	Bio-memristor	ITO-coated glass	Al	ITO	Silk fibroin extracted from cocoons of silkworms	√	19,20
2013	Sericin	ReRAM	Si/SiO_2, PET	Ag	Au	Sericin (M_w = 8000 g/mol)	X	22
2013	Silk fibroin	Bio-memristor	ITO-coated glass	Al	ITO	Silk fibroin-Au nanoparticle blend	√	21
2014	Cellulose nanofiber paper (CNP)	Resistive memory	Si/SiO_2, Al foil	Ag	Pt	CNP-Ag	√	23
2015	Chitosan	ReRAM	Si/SiO_2, PES	Ag	Pt	Chitosan (deacetylation degree 75–85%), chitosan-Ag	X	24
2015	DNA	Bio-memristor	Si/SiO_2	Au	Au	DNA of calf thymus	X	25
2015	Chicken egg albumen	Bio-memristor	ITO-coated glass	Al	ITO	Ovotransferrin, Fe	X	26

clear indication concerning the purity of the memory-inducing compounds. The presence of impurities in natural materials is usually unavoidable even after comprehensive purification steps. Some reports have even revealed that memory-switching effect can only be observed after the natural materials have been added with impurities such as nanoparticles[16,21] and ionic salts.[23,24]

In addition to these natural materials, Aloe vera appears to be a promising candidate for memory application. Although Aloe vera has traditionally used for various medicinal, pharmaceutical, cosmetic, and nutritional purposes,[27-30] its application in electronic devices remains largely unexplored. The demonstrations of living Aloe vera plant towards electrical signals suggest its potential for electronic applications.[31-33] Interestingly, a factory-processed Aloe vera gel (Fruit of Earth Inc, USA) has been investigated as natural dielectric material for electronic applications.[34] Due to its promising dielectric properties, the factory-processed Aloe vera gel is subsequently used as the dielectric layer in an organic field-effect transistor (OFET)[35] with the dielectric properties further verified via theoretical simulation.[36] Recently, memory-switching effects have been concurrently demonstrated in living Aloe vera plant[37] and the factory-processed Aloe vera gel-Au nanoparticle (AuNP) blend.[38,39] Even if the demonstration of memory concept in living Aloe vera plant appears to be impractical for integration into existing electronic manufacturing technologies,[37] it has shed some lights on exploiting the natural material for memory application. An encouraging result has revealed that a write-once-read-many (WORM) memory effect can be induced in a metal/Aloe vera-AuNP/metal device.[38,39] However, the origin of the memory effect was not reported and the role of Au nanoparticles was not specifically elaborated.

In this work, a non-volatile bipolar switching memory effect in natural Aloe vera is reported. To prove the concept of using natural Aloe vera in memory devices, natural Aloe vera gel was extracted from freshly harvested Aloe vera leaves, formulated by additional of ethanol (0–80 wt%), and dried at different temperature (50–120^{o}C). It can be evident that bipolar switching memory effect is induced in the natural Aloe vera layer, as the bottom-up ITO/Aloe vera/Al structure can be repeatedly switched between the low current density OFF-state and high current density ON-state when appropriate voltage sweeps are app lied to the terminals. The current conduction mechanisms pertaining to the memory effect are investigated to gain more insights on the transportation of injected charges across the Aloe vera. The origins of physical charge traps in the Aloe vera layer are proposed to complement the current conduction mechanism. To evaluate

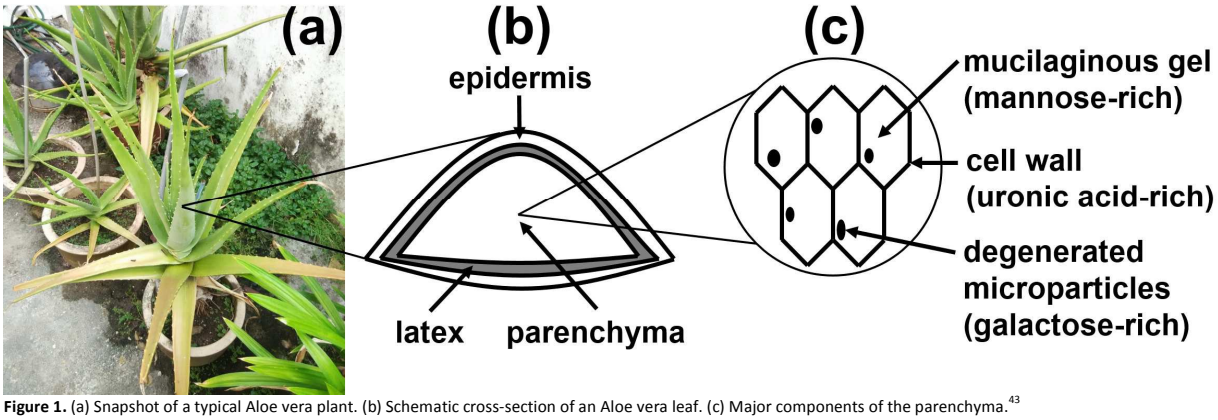

Figure 1. (a) Snapshot of a typical Aloe vera plant. (b) Schematic cross-section of an Aloe vera leaf. (c) Major components of the parenchyma.[43]

the reliability of the memory device, the retention and endurance characteristics of the memory are also measured.

Aloe Vera Leaf Structure and Composition

Aloe vera (*Aloe barbadensis* Miller) is a perennial succulent plant belongs to the Xanthorrhoeaceae family and Asphodeloideae subfamily according to Angiosperm Phylogeny Group III System 2009.[40] Of over 360 Aloe species, Aloe vera is the most common species and is massively cultivated for various medical, pharmaceutical, cosmetic and nutritional purposes.[27-30] The plant is natively grown in tropical and subtropical regions with hot, dry climate. However, due to its enormous commercial values in the aforementioned industries, it has been widely cultivated almost everywhere on the planet. Aloe vera plant has turgid, lance shaped leaves with jagged edges and joined together at the stem resembling a rosette pattern. A snapshot of a typical Aloe vera plant is shown in Figure 1a. As illustrated in Figure 1b, each Aloe vera leaf is composed of three major parts, namely (i) epidermis, (ii) latex layer, and (iii) parenchyma.[41-45] To survive in tropical climate with erratic rainfalls, Aloe vera plant needs to develop a thick outer skin, commonly referred to as epidermis, in order to isolate and prevent loss of water from the leaf. Beneath the epidermis, there is a yellowish, sap-like fluid latex layer that can act as a self-defence mechanism of Aloe vera against herbivores. The innermost part of the Aloe vera leaf is parenchyma, which contains large, colorless, and thin-walled tissues for water storage.

Among the major parts of Aloe vera leaf, parenchyma is of particular importance in this study. It contains around 98.5 wt% of water with the remaining 1.5 wt% mainly composed of carbohydrates, proteins, enzymes, vitamins, minerals, organic acids, phenolic substances, phytosterols, and other compounds.[28-30,41-43] It should be noted that there are significant variations in the chemical composition of parenchyma as reported in the literatures. This discrepancy could probably due to a variety of factors, including the difference in separation techniques, seasonal climate changes, and cultivation conditions.[28-30,41-43] Therefore, the understanding of structural components of the parenchyma in relation to its chemical composition is critical in gaining insights to the chemical changes that may occur during development of Aloe vera-based products. The parenchyma is composed of three distinct structural components (Figure 1c), namely (i) mucilaginous gel, (ii) cell wall, and (iii) degenerated microparticles.[43] The proportions of mucilaginous gel, cell wall, and degenerated microparticles to the parenchyma after moisture removal are 83.1 wt%, 16.2 wt%, and 0.7 wt% respectively.[43] The major fraction of chemical compounds of the three structural components is carbohydrates.[27-30,41-43] Carbohydrates could exist as monomers, oligomers, and polymers in their structural components. When analyzing the content of carbohydrates,[41-43,46] it is always more convenient to reduce the substances to their simplest sugar forms. For example, mucilaginous gel, which is commonly known as Aloe vera gel, contains a large amount of mannose; cell wall is mainly consists of uronic acid, while degenerated microparticles are rich in galactose.[43] In natural living organisms like Aloe vera, most of the carbohydrate substances tend to exist in complex polymers form. Polymeric carbohydrates are often denominated as polysaccharides and they are constructed of more than two sugar units (monosaccharides) linked together by glycosidic bonds. By linking many units of mannose via β-(1,4)-glycosidic linkages, a polysaccharide known as acemannan can be identified as the exclusive carbohydrate substance exist primarily in the Aloe vera gel.[27-30,41-43] Using the same concept, linking the uronic acids together via α-(1,4)-glycosidic bonds, polysaccharide exists in the cell wall can be identified as pectin.[27-30,41-43] By polymerizing galactose, a polysaccharide known as galactan

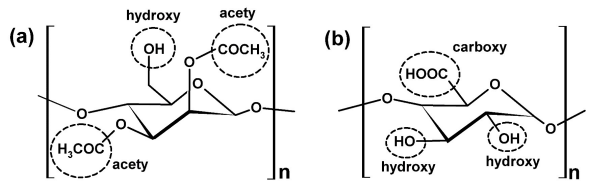

Figure 2. Schematic shows *n*-repeating units of (a) mannose linked by β-(1,4)-glycosidic bonds to form an acemannan and of (b) uronic acid linked by α-(1,4)-glycosidic bonds to form a pectin.[29,46] Function groups at the terminal of the *n*-repeated units for the respective polysaccharides are labelled.

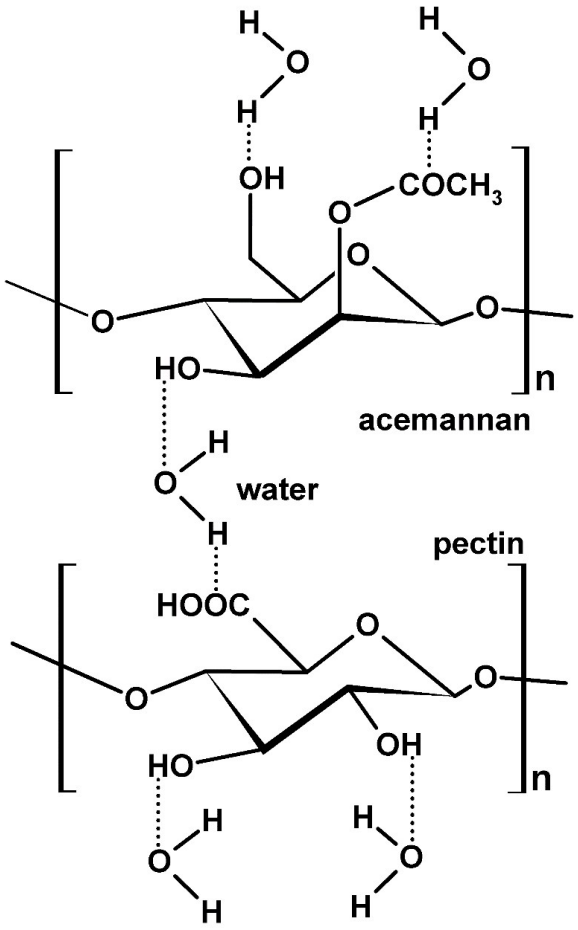

Figure 3. Illustration of hydrogen bonds formation (indicated by dotted lines) between water molecules and acemannan or pectin in an Aloe vera gel.

could be induced as the carbohydrate substance in the degenerated microparticles.[43] Since both Aloe vera gel and cell wall constitute majority (~99.3 wt%) of the structural components in parenchyma,[43] the acemannans and pectins are considered as the most important carbohydrates in an Aloe vera-based memory device for this study.

The chemical structures of both mannose and uronic acid are shown in Figure 2. It can be noticed that a mannose contains a few important functional groups, including hydroxy (−OH) and acety (−$COCH_3$) at the terminals; whereas for uronic acid, function groups that connected to its terminals are hydroxy and carboxy (−COOH). The main role of these functional groups is to provide an interface for the interaction of the respective polysaccharide chain with other molecules via hydrogen bonding due to dipole-dipole attraction force. In the simplest case, a hydrogen bond can be formed between a hydrogen-bond donor and acceptor. An example of hydrogen-bond donor is hydrogen (H) in hydroxy group of a water molecule and hydrogen-bond acceptor is oxygen (O) in covalently bonded carboxy group or in water molecule. In natural Aloe vera, huge amount of water is surrounding the polysaccharides. Therefore, the interaction force (*F*) between two adjunct polysaccharides can be estimated by Coulomb's law (Equation 1)[47] and it is governed by the dipole-dipole interaction of water molecules sandwiched between them with a distance *r* (which is roughly estimated as the diameter of a water molecule) and it is also affected by the relative permittivity (ε_r) of the medium in between the polysaccharides, which is water in this particular situation.

$$F \propto \frac{1}{\varepsilon_r r^2} \quad (1)$$

This hydrophilic nature of polysaccharides is illustrated in Figure 3. The water molecules bounded to acemannan and/or pectin chains by hydrogen bonds could function as a solvation shell.[48] To increase the attraction force and hydrogen bonding between two polysaccharide chains, the distance, *r*, between the chains and the relativity permittivity, ε_r, of the surrounding medium have to be reduced. The former parameter can be reduced by removing of water via heating and drying and the latter one can be modified by introducing solvent such as ethanol with a lower relative permittivity value (ε_r of water and ethanol is 80.4 and 24.3, respectively). By doing so, strengthening of the bonding between polysaccharide chains may lead to solidification and densification of the Aloe vera layer. With this, it may influence its electrical properties.

Experimental

Aloe Vera Gel Preparation

Aloe vera leaves were harvested from a local garden located at Balik Pulau, Penang, Malaysia on the day of experiment. The freshly harvested Aloe vera leaves were between 30 and 50 cm in length corresponding to a 3-year-old plant. The leaves were washed with distilled water to remove dirt. After removing the spikes along the margin, the leaves were cut transversely into pieces and the thick epidermis was carefully separated from the parenchyma by using a sharp blade. The parenchyma was washed extensively with distilled water to remove surface exudate before being homogenized in a food blender (Philips HR2061). The homogenized gel were then centrifuged (Hettich Rotina 38) at 3000 rpm for 30 min to remove fibers. The supernatant was recovered and vacuum filtered through a filter paper (Whatman No. 1) to obtain the Aloe vera gel.

Device Fabrication

The memory test structures were fabricated according to the cross-section shown in Figure 4a. Indium tin oxide (ITO)-coated glass (sheet resistance ≤7 Ω/□, ITO thickness = 220 ± 30 nm) was purchased from Zhuhai Kaivo Optoelectronic Technology Co., China and was used as the substrate for the memory test structure. The substrate was cut into a dimension of 1.5 cm × 1.5 cm by a diamond cutter and was cleaned sequentially with acetone, ethanol, and deionized water in an ultrasonic bath for 30 min, respectively. Spin-coating precursor solutions were prepared by mixing Aloe vera gel with 20, 40, 60, and 80 wt% of absolute ethanol (Merck Millipore, ACS grade). The

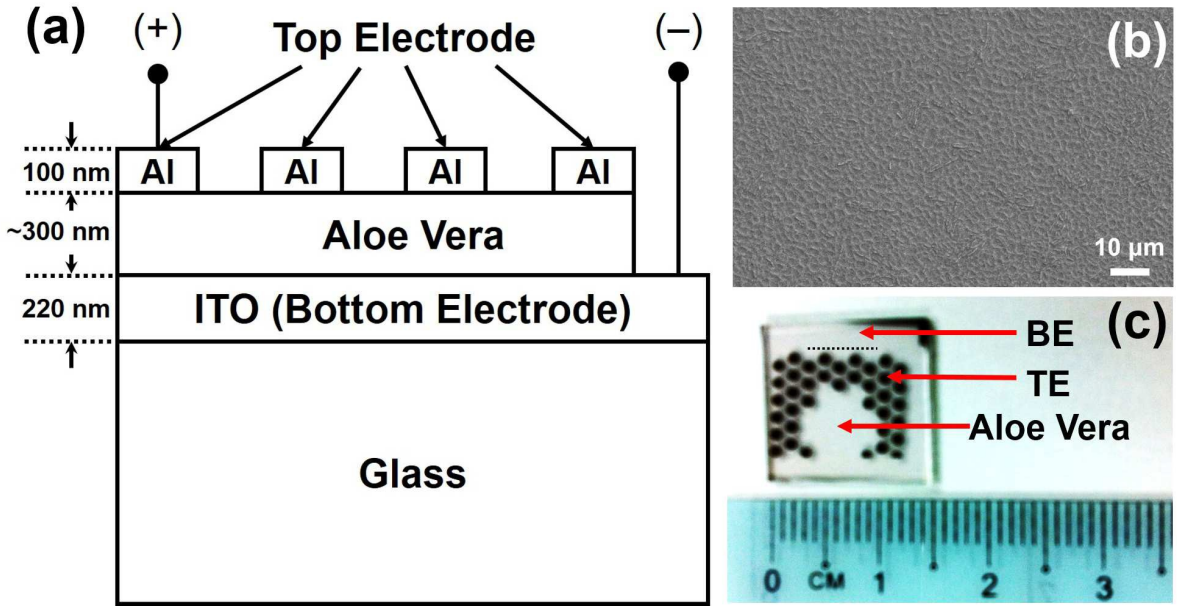

Figure 4. (a) Schematic cross-section of the memory test structure. (b) SEM image of a typical dried Aloe vera surface. (c) Optical image of a complete memory test structure. BE and TE refers to the bottom and top electrodes, respectively.

precursor solutions were spin-coated onto the cleaned ITO glass substrates at 1000 rpm for 30 s. The spin-coated Aloe vera layer was dried on a hotplate at 30°C, 50°C, 80°C, and 120°C for 1 h, respectively. A typical morphology of the dried Aloe vera layer is shown in Figure 4b. Finally, 100-nm thick Al, acting as top electrodes, was thermally evaporated (Quorum Emitech K950X) at a base pressure of approximately 2.25 × 10^{-3} Torr through a metal mask onto the dried Aloe vera layer. A unit of memory device was defined by the area covered by the top electrode. The device area of 5.03 × 10^{-3} cm^2 was in turn defined by the circular patterns (diameter = 0.08 cm) of the metal mask used during evaporation of top electrodes. A complete fabricated test structure is shown in Figure 4c.

Characterization

The thickness of Aloe vera layer was optically measured by a Semiconsoft MProbe20 UVVisSR thin film measurement system. Optical measurement of thickness was usually performed over two steps: (i) measurement of reflectance spectrum of the sample, and (ii) nonlinear curve fitting the measured reflectance spectrum to infer physical properties, such as thickness, of the sample. Before taking any measurements, the system was calibrated by a bare ITO glass substrate with a filmstack structure of void/glass/ITO (bottom to top). The sample was placed at the center of the sample holder (model SS100) and the light probe holder was directly placed on top of the sample to fix the position of incident light source in perpendicular (normal) to the sample surface. The diameter of the light beam was 0.5 cm. The measurement system was controlled via a universal serial bus (USB) by a personal computer (Dell Vostro 2520) preinstalled with TFCompanion v3.95 software. The range of measurement wavelength was set to 250–850 nm to encompass both UV and visible range of electromagnetic radiation. For each measurement, 10 reflectance readings were recorded and the average value of these reflectance readings was considered for thickness calculation. The measured reflectance spectrum of the bare ITO glass substrate is shown in Figure 5a. The optical properties which include refractive index (*n*) and extinction coefficient (*k*) of the ITO layer were taken from the library and were shown in Figure 5b. By setting the initial thickness values to 220 nm, which is the nominal ITO thickness provided by the manufacturer, the actual thickness of the ITO layer can be inferred by curve fitting the measured reflectance spectrum according to Levenberg-Marquardt algorithm.[49] The goodness of fit is given by

$$\chi^2(\hat{a}) = \sum_{i=1}^{N}\left[\frac{r_i - r(\lambda_i;\hat{a})}{\sigma_i}\right]^2 \quad (2)$$

where *i* is the number sequence, *N* is the total number of measured reflectance, $\hat{a}$ is a vector of parameters such as thickness, *n*, and *k*, λ_i is the *i*-th wavelength, r_i is the *i*-th measured reflectance, $r(\lambda_i;\hat{a})$ is the calculated reflectance based on the filmstack model, and σ_i is the *i*-th standard deviation. The smaller the χ^2 value, the better the curve fit. Thus, the inferred ITO thickness of 219.51 ± 0.22 nm is very close to the nominal thickness provided by the manufacturer, as indicated by χ^2 = 0.3567. The confidence interval of ±0.22 nm is based on 99% confidence level set for the thickness calculation.

The surface morphology of the dried Aloe vera layers was investigated using a field-emission scanning electron microscope (FE-SEM) (Zeiss Leo Supra 50 VP). Before characterization, the samples were sputtered with a thin (~5 nm) gold layer to avoid electron charging effect during FE-SEM

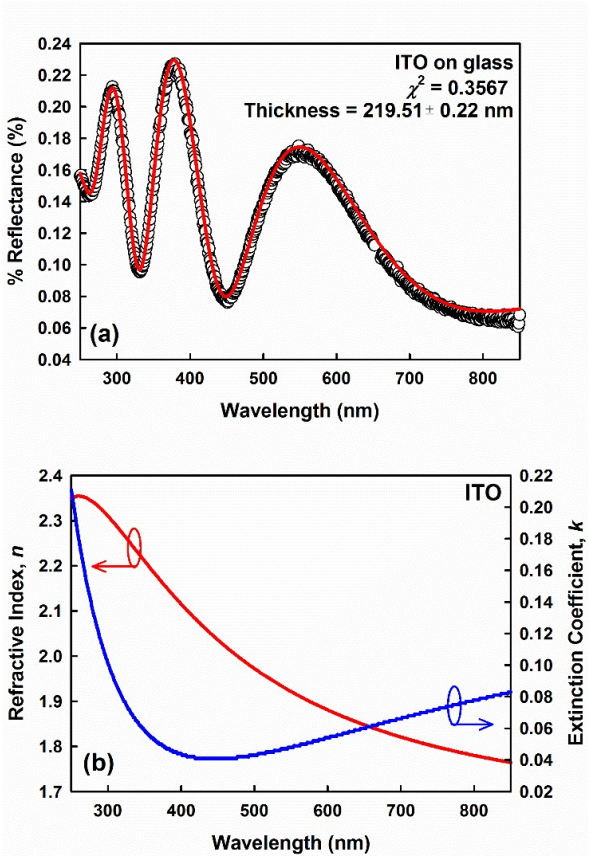

Figure 5. (a) The measured reflectance spectrum of the bare ITO glass substrate. Open symbol represents the measured reflectance and solid line represents the fitted curve. (b) Refractive index and extinction coefficient used to model the optical properties of the ITO layer.

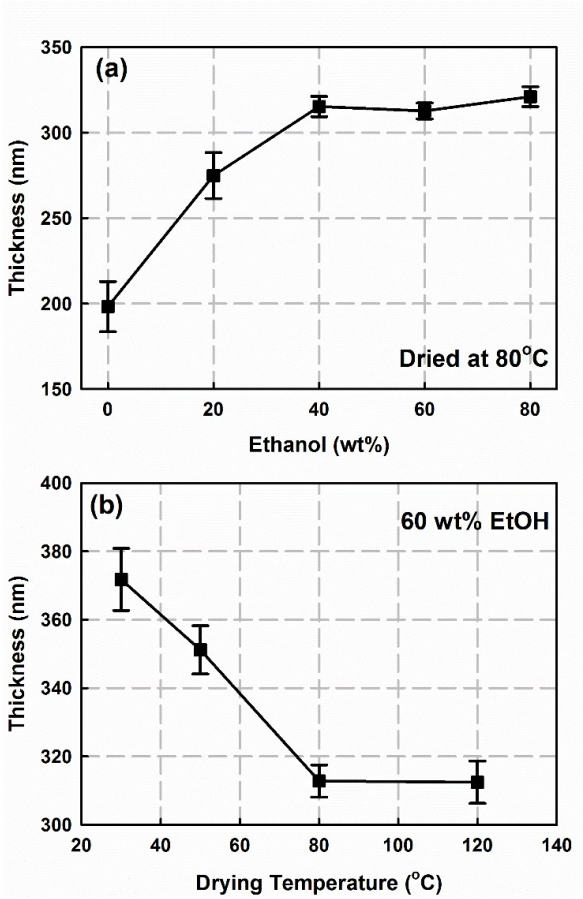

Figure 6. Typical thickness of Aloe vera layer as a function of (a) ethanol content in the precursor dried at 80°C and (b) drying temperature for Aloe vera gel with 60 wt% of ethanol. The error bars represent confidence interval based on a 99% confidence level statistical distribution to a total of 600 thickness values inferred from measured reflectance of wavelength from 250 to 850 nm with a resolution of 1 nm.

characterization. The gold-coated samples were then fixed on metallic stubs using a conductive carbon tape and placed into the vacuum chamber of the microscope for image capturing.

To identify the chemical structures of compounds present in Aloe vera, Fourier Transform Infrared Spectroscopy (FTIR) spectra of dried Aloe vera samples were acquired using a spectrometer (Perkin Elmer Spectrum 1). The samples were prepared by casting pure Aloe vera gel onto a petri dish, left to dry on a hotplate at 30, 50, 80, and 120°C before being scratched out using a spatula. The dried Aloe vera samples were blended with KBr (Merck, spectroscopy grade) in a ratio of 1:10 and pressed into pellets. A background scan was performed using a void pellet holder prior actual spectrum acquisition. For each samples, a spectrum was recorded in transmittance mode from 4000 to 400 cm^{-1} with a resolution of 4 cm^{-1} for a total of 32 times.

The effects of heating temperature on the weight loss of Aloe vera gel were examined by thermogravimetric analysis (TGA). In a typical measurement, Aloe vera gel was put into an alumina heating pan in the measurement chamber of a Mettler Toledo STAR1 thermogravimetric analyzer and TGA was carried out under heating rates of 5°C/min, 10°C/min, and 20°C/min. The weight loss of Aloe vera gel was measured from room temperature to 200°C in nitrogen ambient with a flow rate of 10 mL/min.

To investigate the electrical properties of the dried Aloe vera layer as an active memory switching material, current-voltage characteristics of the test structures (Figure 4c) was measured by an Agilent 4156C Precision Semiconductor Parameter Analyzer, which was controlled via a general purpose interface bus (GPIB) by a personal computer (HP Compaq nc2510) preinstalled with Metrics ICS v3.6 software. The samples are placed inside a Lake Shore TTP4 cryogenic probe station equipped with four probe arms and a vacuum chuck. All measurements were performed at ambient conditions with the bias voltage applied on the top Al electrode and the bottom ITO electrode grounded at all time.

Results and Discussion

The potential use of Aloe vera for memory device often involves formulation of extracted Aloe vera with ethanol and then undergoes some basic processing steps, such as drying

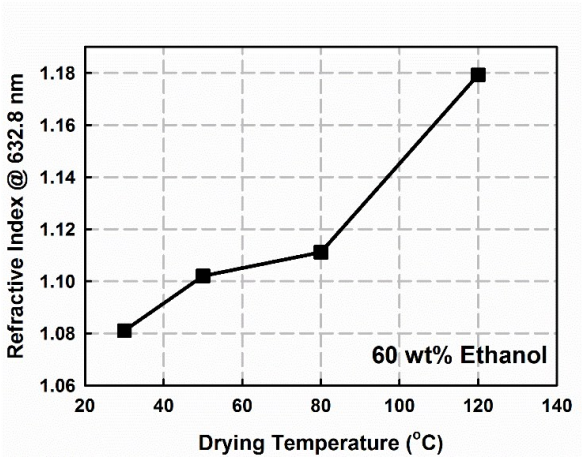

Figure 7. Refractive index of Aloe vera layer with 60 wt% of ethanol as a function of drying temperature.

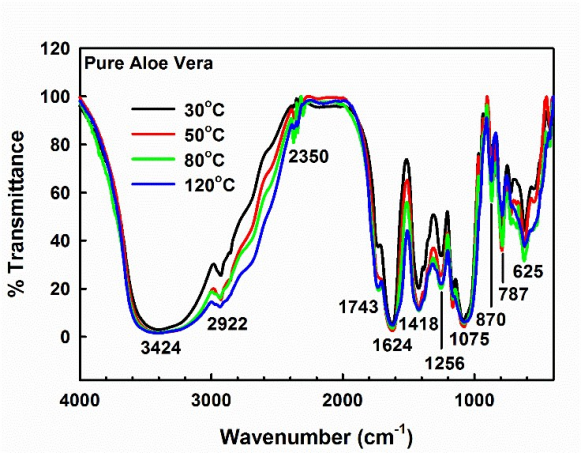

Figure 8. FTIR spectra of pure Aloe vera layer dried at 30, 50, 80, and 120°C.

and heating, so that a dried Aloe vera layer can be deposited from the formulated solution precursors. Memory device developed from solution process is more appealing than the memory concept demonstrated in living Aloe vera plant[37] because it can be readily integrated into existing electronic manufacturing technologies. The effects of ethanol on thickness of the Aloe vera layer on ITO glass substrate after being dried at 80°C are presented in Figure 6a. The thickness increases approximately 38.72% from 198.24 ± 14.70 to 274.98 ± 13.48 nm as 20 wt% of ethanol is being added to the pure Aloe vera gel. The thickness of Aloe vera with 40 wt% of ethanol is 315.35 ± 5.97 nm, which is an increment of about 14.68% from Aloe vera with 20 wt% of ethanol. With the addition of 60 and 80 wt% of ethanol into pure Aloe vera gel, the thicknesses are recorded as 312.80 ± 4.69 nm and 321.13 ± 5.83 nm, respectively. It can be observed that thickness of Aloe vera layer increases steadily as the ethanol concentration in Aloe vera is increased from 20 to 60 wt%. This increasing trend is eventually flattened off beyond 60 wt% of ethanol.

The variations of Aloe vera film thickness as a function of drying temperature with 60 wt% of ethanol added in the pure Aloe vera deposited on ITO glass substrate are presented in Figure 6b. It can be observed that the film thickness decreases 5.54% from an initial value of 371.8 ± 9.09 to 351.2 ± 7.05 nm as the drying temperature is increased from 30°C to 50°C. The film thickness is further decreased as the drying temperature increases to 80°C. Further increment in drying temperature from 80°C to 120°C does not affect much of the film thickness. This is because vaporization temperature of ethanol is approximately 78°C and beyond that ethanol is fully vaporized. Besides, water as a main constituent in Aloe vera is also able to be slowly vaporized as the drying temperature is approaching the boiling temperature of water (100°C). As a result, a compact layer of dried Aloe vera is produced. The detail explanation of the effects of drying temperature and concentration of ethanol on the weight loss of Aloe vera gel in terms of chemical composition and structural change will be presented later.

The refractive index values of Aloe vera layer with 60 wt% of ethanol deposited on ITO glass substrate and dried at different temperature are shown in Figure 7. The refractive index increases monotonically from approximately 1.08 to 1.18 as the drying temperature increases from 30°C to 120°C. This increment may be due to solidification of the Aloe vera gel and causing a denser dried Aloe vera layer with more compact structure. This can be explained by the role of ethanol and water affecting pectin and acemannan in the Aloe vera gel as the drying temperature increases. The detail mechanism will be discussed in the subsequent paragraphs.

Figure 8 shows the FTIR spectra of pure Aloe vera dried at different temperatures (30, 50, 80, and 120°C). All samples exhibit a broad absorption band centered at 3424 cm^{-1}, which is due to the stretching of –OH groups, a characteristic of carbohydrate monomers, including mannose and uronic acid.[50-55] The absorption band at 2922 cm^{-1} can be assigned to the symmetrical and asymmetrical C–H stretching of aliphatic –CH and $–CH_2$ groups. The absorption band at 1743 cm^{-1} is a characteristic of C=O stretching, indicating the presence of carbonyl groups in Aloe vera samples. The absorption peaks at 1634 and 1418 cm^{-1} are associated respectively to the asymmetrical and symmetrical $–COO^-$ stretching of carboxylate compounds in Aloe vera. The absorption peak at 1256 cm^{-1} corresponds to the C–O–C stretching of $–COCH_3$ groups. The absorption peak at 1075 cm^{-1} may be due to C–O stretching associated to rhamnogalacturonan, a side-chain constituent of pectins. The absorption peak at 870 cm^{-1} is due to C–H out-of-plane deformation of carbohydrate monomers. These absorption peaks indicate the presence of mannose and uronic acids, as well as their carbohydrate polymers, i.e. acemannans and pectins.[42,45,50,51]

The intensity of absorption peaks can reveal the changes in chemical structure of acemannan and pectins. Specifically, the decrease in peak intensities at 1743 and 1256 cm^{-1} with increasing temperature is corresponding to the deacetylation of acemannans. The decrease in infrared intensities as the Aloe vera underwent pasterurization has also been reported[42,45] and the result is consistent with glycosidic

linkage,[42,45] colorimetry,[56] and mass spectrometry.[57] Figure 9 illustrates the deacetylation of an acemannan chain. The process has a profound effect on the interactive properties of acemannans. With the removal of $-COCH_3$ groups, the separation distance between the force of two molecules is reduced (Equation 1), leading to the formation of hydrogen bonds. This deacetylation process may also lead to the solidification of Aloe vera layer with increasing drying temperature.[58] Besides that, the absorption peaks at 1743, 1624 and 1418 cm^{-1} are the characteristics of pectins in Aloe vera, due respectively to C=O stretching of carboxylic ester ($-COOCH_3$), asymmetrical and symmetrical $-COO^-$ of carboxylic acid (–COOH) groups.[54,55,59,60] Intensity reduction at 1743 cm^{-1} as drying temperature increases indicates that pectins has undergone some structural changes. Specifically, the intensity reduction at 1743 cm^{-1} suggests the increasing presence of $-COOCH_3$ groups in pectin terminals as the Aloe vera is dried at higher temperatures. Nevertheless, the larger peak intensities at 1624 and 1418 cm^{-1} regardless of the drying temperature lead to the conclusion that low methoxyl pectins (i.e. pectins with more –COOH groups)[61-63] are the dominant pectin species in the Aloe vera.

The heating rate has a pronounced effect on the weight-loss characteristics of Aloe vera gel. Figure 10a shows the weight-loss characteristics of pure Aloe vera gel heated at different rates (5°C/min, 10°C/min, and 20°C/min) and measured by a thermogravimetric analyzer. It is important to note that weight-loss characteristics differ significantly when being heated at different rates. The temperature of which the weight of pure Aloe vera gel reduces to approximately 0% is decreased as the heating rate increases. In this study, the slowest rate (5°C/min) may allow the temperature to transfer into the internal part of the gel more uniformly so that changes of weight due to any thermal event can be recorded in a wider temperature range. Therefore, for the subsequent TGA characterization, heating rate of 5°C/min has been used.

Pure Aloe vera gel mixed with 0, 20, 40, 60, and 80 wt% of ethanol in solution were characterized by TGA and the results are shown in Figure 10b. From the five samples, three distinct weight-loss characteristics can be observed with pure Aloe vera (0 wt% ethanol) as one group, Aloe vera gel with 20 wt% ethanol as another, and Aloe vera gel with ethanol of 40 wt% and higher as the last group. For pure Aloe vera gel (0 wt% ethanol), a weight loss from original 100.0% to 89.3%, corresponding to the temperature ranges from 37°C to 60°C, can be observed. This minor weight loss is probably caused by the structural modification of pectin backbone. In this stage, pectin may undergo the process of de-esterification, creating the negatively charged $-COO^-$ groups in its structure while releasing methanol molecules and protons,[64-66] as shown in Figure 11a. Furthermore, the de-esterification could be catalyzed by the pectinmethylesterase (PME) enzymes exist endogenously in Aloe vera gel [65,66]. The optimal temperature for PME activity varies between 45°C and 55°C and the enzymes denature at higher temperatures.[65,66] The process of de-esterification could be further supported by the FTIR spectra (Figure 8) with the presence of strong bands at 1624 and 1418 cm^{-1} due respectively to asymmetrical and symmetrical stretching of the –COOH groups in Aloe vera mixed with 60 wt% of ethanol and dried at different temperatures.

Following that, a more drastic weight loss of the pure Aloe vera gel from 89.3% to 21.5% corresponding to temperatures range between 60°C and 90°C can be observed. The weight

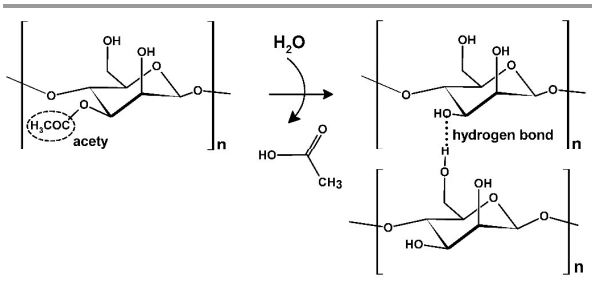

Figure 9. Schematic illustration of deacetylation process. The acetyl group of a mannose constituting the backbone of acemannan is removed leading to the formation of a new hydrogen bond with another acemannan chain.[42,45]

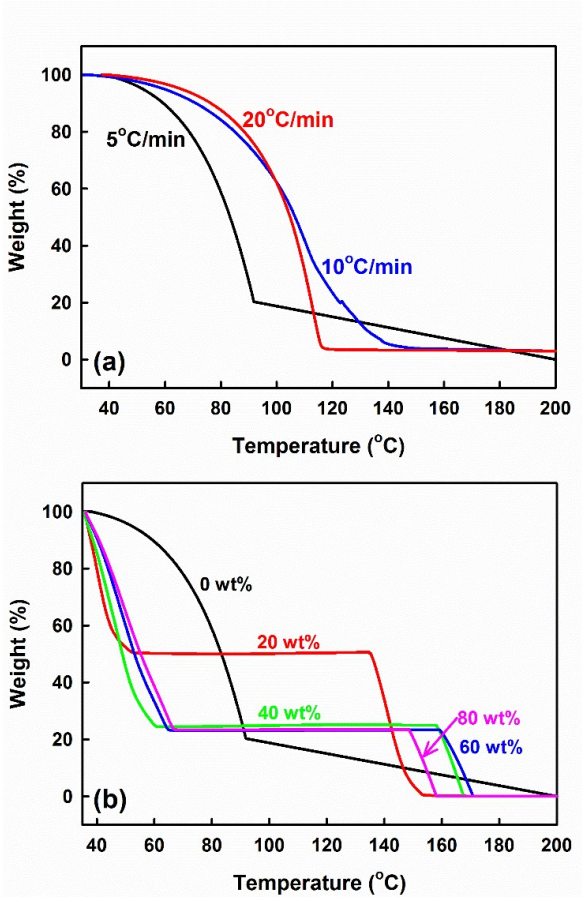

Figure 10. Percentage weight losses as a function of temperature for (a) pure Aloe vera gel heated at different rates (5°C/min, 10°C/min, and 20°C/min) and (b) precursors with different amount (0, 20, 40, 60, and 80 wt%) of ethanol added in Aloe vera gel measured by a thermogravimetric analyzer.

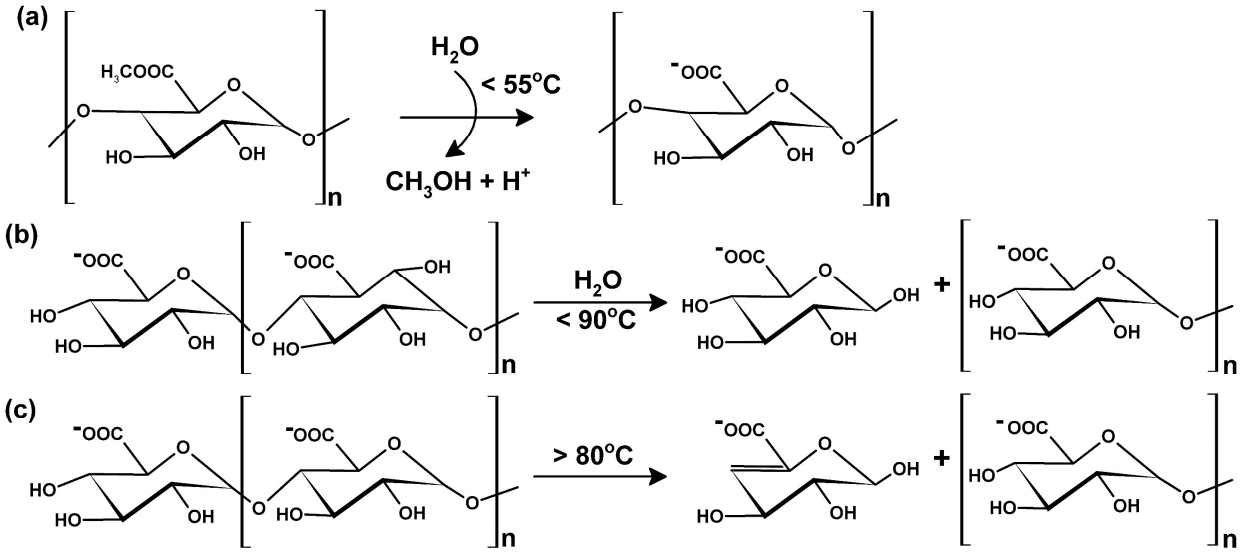

Figure 11. Schematic of (a) de-esterification, (b) hydrolysis, and (c) β-elimination reaction of pectin. Processes (a) and (b) may occur up to temperature of approximately 55°C[65,66] and 90°C,[68-70] while process (c) may be initiated at temperature higher than 80°C.[42,45,63,67]

loss may due to a multitude of physical and chemical changes of the pure Aloe vera gel. One of the main causes may be attributed to the water-assisted breaking up of pectin chain into simpler uronic acids.[42,45,67] The process is named as hydrolysis and is schematically shown in Figure b. This process could also be catalyzed by another cell-wall modifying enzymes known as polygalacturonase (PG) exist endogenously in Aloe vera gel.[68,69] During hydrolysis, the α-(1,4)-glycosidic bond connecting two uronic acids together is cleaved by addition of a water molecule, leading to the breaking up of the longer molecular chain of polysaccharide into a shorter one. Heating at temperatures above 90°C could inactivate the PG enzymes and eventually slow down the hydrolysis process.[70] In addition to enzymatic degradation, heating at high temperatures (>80°C) could also promote degradation of pectin via β-elimination reaction, which refers to the cleavage of glycosidic linkages between the uronic acid residues and release of a non-saturated uronic acid molecule from a pectin chain as illustrated in Figure 11c.[42,45,67] The degradation of pectin chains is probably the main cause leading to weight loss of the pure Aloe vera gel at temperatures ranging from 37°C to 90°C.

In comparison, the acemannan chains are less susceptible to the effects of temperature.[42,45] Nevertheless, the specific polysaccharide chains could undergo structural modification when the gel is subjected to heating above 60°C.[42,45] The deacetylation process tends to become significant as the temperature increases and contributes to the formation of hydrogen bonds between different acemannan chains.[42,45] Consequently, a compact and firm polysaccharide network may be formed in the partially dried pure Aloe vera gel. As the temperature is increased beyond 90°C, water molecules, including those bounded to the polysaccharide chains in the form of solvation shells, are being removed. This dehydration process may either form a longer chain of polysaccharide of acemannan (Figure 12a) and/or form a cross-linked and branched polysaccharide network with mannose or uronic acid residues (Figure 12b). Due to its size and weight, the strong and firm polysaccharide network formed by dehydration is temperature resistance. Only by increasing the temperature to approximately 200°C, a total decomposition of the polysaccharide network, including its backbone molecules, may occur as shown in the weight loss of TGA result in Figure 10.

The weight-loss characteristic of Aloe vera gel mixed with 20 wt% ethanol differs significantly from the weight-loss characteristics of the pure Aloe vera gel. A weight loss from original 100.0% to 52.3% occurs between 37°C and 50°C. It is 45.5% higher if compared with the weight loss of pure Aloe vera gel within the same temperature range. This higher rate of weight loss may probably due to de-esterification of pectin chains. The de-esterification process seems to be promoted by the addition of 20 wt% of ethanol into to the Aloe vera gel. This fact could be explained by referring to Equation 1. With the addition of ethanol, attraction force between a pectin and a PME enzyme is increased, due to the lower value of relative permittivity (ε_r = 24.3) of ethanol if compared to water (ε_r = 80.4). Consequently, the PME enzymes may be attracted to the pectin chain and a catalyzed process of de-esterification takes place. The weight loss of this sample begins to stabilize at temperatures above 50°C, partly because of the retardation of pectin de-esterification as PME enzymes has been denaturalized. In contrast to PME enzymes, the addition of ethanol seems to have negatively affected the activities of PG enzymes,[61-63] as hydrolysis of pectin chains ceases to occur. Furthermore, the degradation of pectin chains due to β-elimination reaction promoted by heating at temperatures above 80°C is also suppressed by the addition of ethanol.[61-63] Similar observations in which heat inactivation of cell wall tissues of fruits and vegetables in the presence of ethanol may

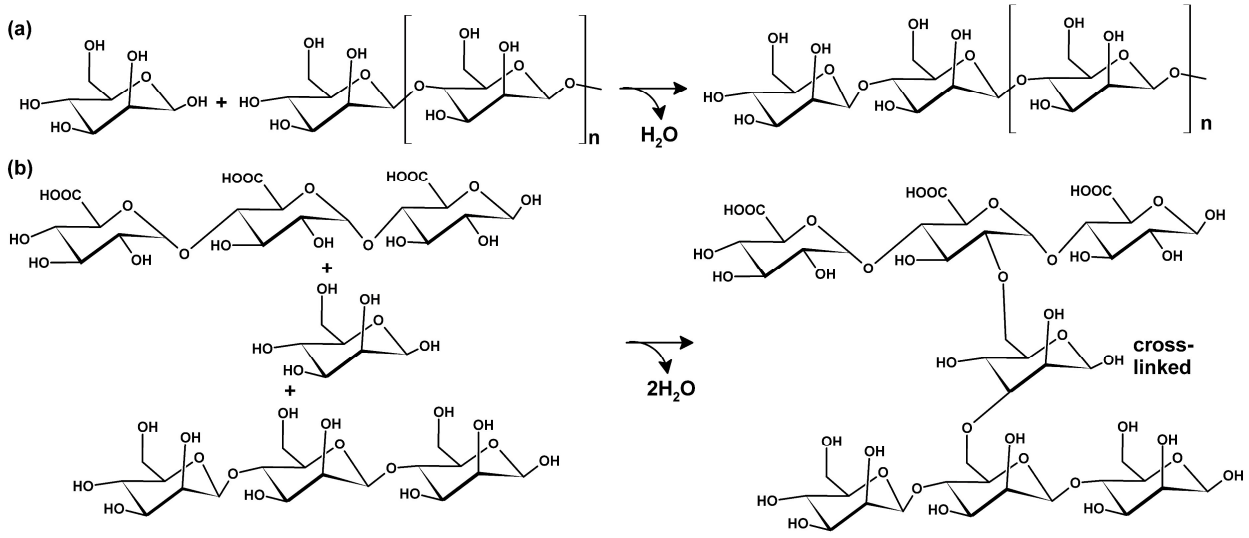

Figure 12. Schematics of dehydration process in polysaccharide to create a (a) longer and (b) cross-linked and branched polysaccharide network.

preserve the pectin chains from degradation via β-elimination reaction has been reported.[61-63] On the other hand, the process of deacetylation of acemannan chains is initiated at temperatures above 60°C.[42,45] The deacetylated acemannan chains together with de-esterified pectin chains, leads to the formation of stable, thermally resistance substance, in which the polysaccharide chains interact with each other via the formation of hydrogen bonds. The combined polysaccharide substances are stable throughout the temperatures ranging from 50°C to 134°C. As the temperature is increased beyond 134°C, weight of the sample is reduced significantly from 50.1% to 1.4%. This weight loss is mainly due to dissociation of the substance into individual polysaccharide chains follows by breaking of its backbone molecules and eventually totally burning off at 154°C.

As the ethanol content in Aloe vera gel is increased to 40, 60, and 80 wt%, another group of weight-loss characteristics could be observed. All of the samples recorded an initial weight loss from 100.0% to about 24.8% corresponding to temperatures range from 37°C to 60°C. In this stage, the rapid weight reduction rate of the samples is similar to the sample with 20 wt% of ethanol. Therefore, the similar pectin de-esterification process that causes the weight loss in this range of temperatures may also be applicable. Unlike the sample with 20 wt% of ethanol, these samples exhibit drastic weight losses up to a higher temperature (60°C) with a relatively lower weight of stabilization. These differences may be due to the effect of ethanol on PG enzymes, which function is to catalyze the hydrolysis of pectin chains. While 20 wt% of ethanol may be the optimal concentration to inhibit activities of the enzymes, over-addition of ethanol could lead to the adverse effect.[61-63] Thus, the parallel occurrence of enzymatic de-esterification and hydrolysis leads to the lower weight of stabilization observed in these samples. As the temperature is increased above 60°C, enzymes in the samples denature and the weight loss due to de-esterification and hydrolysis of pectin chain are slowing down, leading to the observed weight stabilization. Due to the addition of ethanol, further degradation of pectin chains via β-elimination reaction is suppressed. The pectin chains interact with the deacetylated acemannan chains via hydrogen bonds to create a stable, thermally resistance polysaccharide substance. This leads to the densification of the samples and it is in agreement with the monotonically increase of refractive index as shown in Figure 7. Additionally, the stabilized weight of the samples can be maintained up to a certain temperature that is higher than sample added with 20 wt% of ethanol. Specifically, the stabilized weight of the sample with 40, 60, and 80 wt% of ethanol can be maintained up to 157°C, 158°C, and 148°C, respectively. This observation indicates that by adding an appropriate concentration of ethanol stabilization of weight in the Aloe vera could be extended accordingly. Based on literatures, the extended weight stabilization is attributed by three positive effects when ethanol is added in the Aloe vera gel, namely (i) to increase de-esterification of pectin due to enhancement of interaction between pectin and PME enzymes,[65,66] (ii) to reduce hydrolysis process due to inhibit activities of PG enzymes,[61-63] and (iii) to prevent β-elimination.[61-63]

The switching effect of a memory device can be examined from a test structure (Figure 4a) and a typical current density–voltage (*J*–*V*) characteristic of the device with pure Aloe vera dried at 50°C is presented in Figure 13. In a typical measurement, a sweeping voltage is applied on the top electrode and the magnitude of current that flows through the device is recorded. The current density (*J*) was computed by dividing the current (*I*) over area of top electrode (*A*). The ultimate aim of this figure is to define typical terminologies and parameters used to describe a memory device in this study. As the applied voltage is swept from 0.0 to −0.9 V (sweep 1), a relatively low current density ranging from 10^{-7} to 10^{-2} A·cm^{-2} is recorded. This level of current density is defined as OFF-state (or high-resistance state, HRS). Beyond −0.9 V, an abrupt increment in current density from 10^{-2} to 10^{1} A·cm^{-2} is

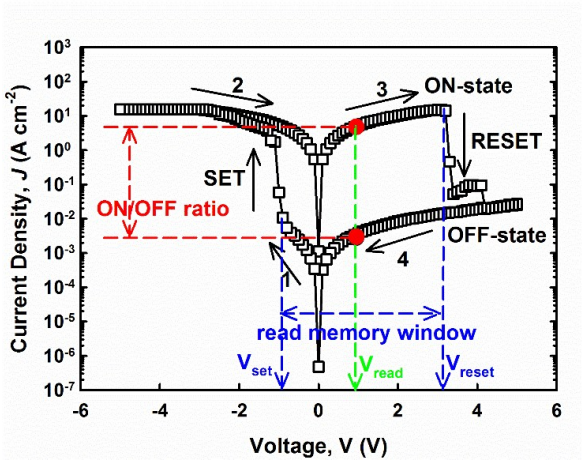

Figure 13. A typical current density–voltage (J–V) characteristic of an Aloe vera-based memory device. Vset, Vreset, and Vread refer to the threshold voltage of SET process, threshold voltage of RESET process, and read voltage used to probe the status (ON- or OFF-state) of the memory device, respectively.

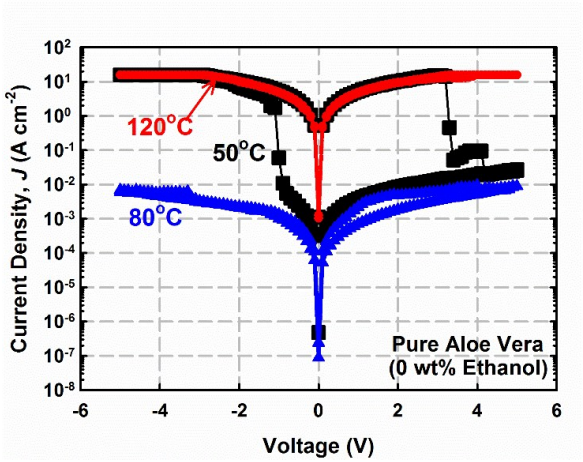

Figure 14. A family plot of J–V characteristics of test structures based on pure Aloe vera (0 wt% ethanol) dried at 50°C, 80°C and 120°C.

detected and this high current-density level is defined as ON-state (or low-resistance state, LRS). The transition from the initial OFF- to ON-state is termed as SET, which could serve as the "writing" process of a memory device and the threshold voltage for this setting or writing process that cause an abrupt increment in current density is known as set voltage, V_{set}. Once the transition occurs, the device stays in its ON-state, even if the applied voltage is swept from V_{set} to −5.0 V. Subsequently, a reverse voltage (sweep 2) is swept from −5.0 to 0.0 V. The device remains relatively stable in the ON-state with a high level of current density (~10^{1} A·cm^{-2}) flowing through it. As the reverse sweeping voltage reaches 0.0 V, a considerable drop in the current density is recorded. Nevertheless, this current density level is still approximately 4 orders of magnitude larger than the original current density value at 0.0 V before the bias. This indicates that even at flatband voltage, the charges are able to be stored in the Aloe vera layer.

When the applied voltage is further swept positively from 0.0 V (sweep 3), a dramatic increment in current density to a much higher value is recorded. This shows that the device is remaining in the ON-state. This state remains stable until the sweeping voltage approaches a forward bias of 3.1 V, where a sudden drop in the current density from approximately 10^{1} to 10^{-3} A·cm^{-2} corresponding to ~10^{4} orders of magnitude difference, can be observed and now the device is being switched back to the OFF-state. This transition from the ON- to OFF-state in forward bias direction is termed as RESET, which could serve as the "erasing" process of a memory device. The threshold voltage in which a remarkable reduction in current density is known as reset voltage, V_{reset}. After the transition, the device continues to stay in its OFF-state even if the applied voltage is further swept from V_{reset} to 5.0 V. The current density remains at a low level ranging from 10^{-2} to 10^{-4} A·cm^{-2} when the voltage is swept from 5.0 V back to and approaching 0.0 V, indicating that the device is stable in the OFF-state. At 0.0 V, the device is still in the OFF-state but the value of current density is drastically reduced back to its original value, i.e. ~10^{-7} A·cm^{-2}. Since V_{set} and V_{reset} of the device are of opposite polarity, this kind of *J–V* characteristic is also called bipolar memory switching. The status of the memory device can be read at any time by applying a read voltage (V_{read}) within the read-memory window that is in between V_{set} and V_{reset}. A large read memory window allows more flexibility in designing the probing circuitry, as the status of memory device can be read over a wider range of voltage without risking the change of memory state during the "reading" process. Additionally, the read-memory window is somewhat constrained by trading off in the design of an external probing circuit that requires V_{read} to be larger than one tenth of the magnitude of V_{set}.[71] Therefore, V_{read} is fixed at 1.0 V in this study. Another important parameter of the memory device is ON/OFF ratio. This ratio compares the ON- to OFF-state of current density at V_{read}. A high ON/OFF ratio is highly desirable to avoid erroneous probing of a memory status. Although a small ON/OFF ratio of about 1.2 is sufficient to be detected by a sophisticated probing circuitry, ON/OFF ratios of >10 are required to ensure effective status reading by any conventional probing circuitry.[71]

The *J–V* characteristics of test structures based on pure Aloe vera (0 wt% ethanol) are found to be strongly dependent on the drying temperature. Figure 14 presents a family plot of *J–V* characteristics for the test structures with pure Aloe vera dried at 50°C, 80°C, and 120°C. Each of the test structures shows a different *J–V* characteristic curve. Of the test structures, it can be noticed that only the test structure dried at 50°C exhibits a *J–V* characteristic curve with bipolar resistive effect, which can be utilized for memory application. The test structure is switched from its initial OFF- to ON-state at V_{set} = –0.9 V and it remains in the ON-state until V_{reset} = 3.1 V is applied. The memory device features an ON/OFF ratio of approximately 10^{3} at V_{read} = 1.0 V and a read-memory window of 4.0 V. In contrast, no obvious memory switching effect can be observed from the *J–V* characteristics of the pure Aloe vera dried at 80°C and 120°C. The test structure with pure Aloe vera dried at 80°C records a low level of current density ranging

Table 2. Conduction mechanisms of memory devices based on natural materials and the characterization techniques used to investigate and to confirm the conduction mechanisms.

Natural material	Characterization techniques			Conduction mechanism	Source of filament-forming species	Ref.
	Chemical	Electrochemical	Electrical			
Tobacco mosaic virus	√	X	√	Charge trapping/detrapping in Pt nanoparticles	No formation of filament being reported	16
Ferritin	√	√	√	Formation and rupture of Fe ions-based filament	Composition of natural materials	17
Lysozyme	X	√	√	Formation and rupture of filament as charge trap and detrap in LYS/PSS layers	Composition of natural materials	18
Silk fibroin	X	√	√	Formation and rupture of silk fibroin-based filament	Composition of natural materials	19,20
Sericin	X	√	√	Charge trapping/detrapping in sericin	No formation of filament being reported	22
Silk fibroin	√	X	√	Formation and rupture of silk fibroin- and AuNPs-based filament	Composition of natural materials	21
Cellulose nanofiber paper	X	X	√	Formation and rupture of Ag-based filament	Ions dissolved from top electrode	23
Chitosan	X	√	√	Formation and rupture of Ag-based filament	Ions dissolved from top electrode	24
DNA	√	X	√	Charge trapping/detrapping in DNA layers	No formation of filament being reported	25
Chicken egg	√	X	√	Formation and rupture of Fe ions-based	Trace minerals of natural	26

from 10^{-7} to 10^{-2} A·cm^{-2} throughout the entire range of the voltage sweeps. Whereas, a high level of current density ranging from 10^{-3} to 10^{1} A·cm^{-2} is recorded in the test structure with pure Aloe vera dried at 120°C throughout the entire range of the voltage sweeps. The respective low and high level of current density are close to the respective OFF- and ON-state of their counterpart with pure Aloe vera dried at 50°C. The difference in the J-V characteristics has been supported by the FTIR spectra of Aloe vera dried at varying temperatures (Figure 8). Changes in chemical structures such as deacetylation of acemannans and de-esterification of pectins may be the reasons behind the difference in the observed J-V characteristics.

Several conduction mechanism such as Schottky emission,[15,72] Poole-Frenkel emission,[15,73,74] Fowler-Nordheim tunneling,[75,76] filamentary conduction,[24,77-79] ionic conduction,[79-81] conformational change conduction,[82-84] and space-charge-limited conduction (SCLC)[85-89] have been established to describe the charge transport in insulator/semiconductor systems. Owing to the progress in organic materials as active and passive layers of electronic devices in recent decades, these mechanisms have also been adapted to elucidate the charge conduction process in organic electronics this includes devices fabricated from natural materials. Table 2 lists out the memory devices based on natural materials and their corresponding conduction mechanisms. Of these conduction mechanisms, the resistive switching phenomena of natural materials are mainly attributed to charge trapping/detrapping processes. In general, organic materials unlike their inorganic counterparts in that their energy bands are loosely defined by the highest occupied molecular orbitals (HOMO) and lowest unoccupied molecular orbitals (LUMO) with the presence of localized energy states for charge trapping/detrapping process. These localized states may originate from polymer chain ends, chain interfaces, bulk and surface dipoles, amorphous-crystalline boundaries, or impurities in the materials.[15] More specifically, trapping/detrapping of electrons in TMV,[16] sericin,[22] and DNA layers[25] have been proven experimentally and the resultant resistive switching have been realized in memory devices.

There are also literatures (Table 2) reported that resistive switching memory of some natural materials is controlled by the formation and rupture of conductive filaments. In fact, the formation of conductive filaments requires charges to be trapped/detrapped within the active layer of natural material. During the process of filament formation, supplied electrons are being trapped/detrapped in localized states of the active layer. In particular, these localized states are chemically active sites within the natural materials and the process of electron trapping/detrapping can be viewed as oxidation and reduction (redox) process that involves a specific compound of the natural materials. Of the memory devices based on natural materials (Table 2), three sources of filament-forming species can be identified, namely from (i) the composition of the natural materials (regardless of original composition or intentionally incorporated species), (ii) trace minerals of the natural materials, and (iii) ions dissolved from top electrode. Overall, the formation and rupture of localized filaments have been evidenced by three major types of characterization techniques, namely (i) chemical, (ii) electrochemical, and (iii) electrical measurements. Specifically, the chemical techniques including time-of-flight secondary ion mass (TOF-SIM) spectroscopy, X-ray photoelectron spectroscopy (XPS), Raman spectroscopy, and FTIR were employed to investigate the

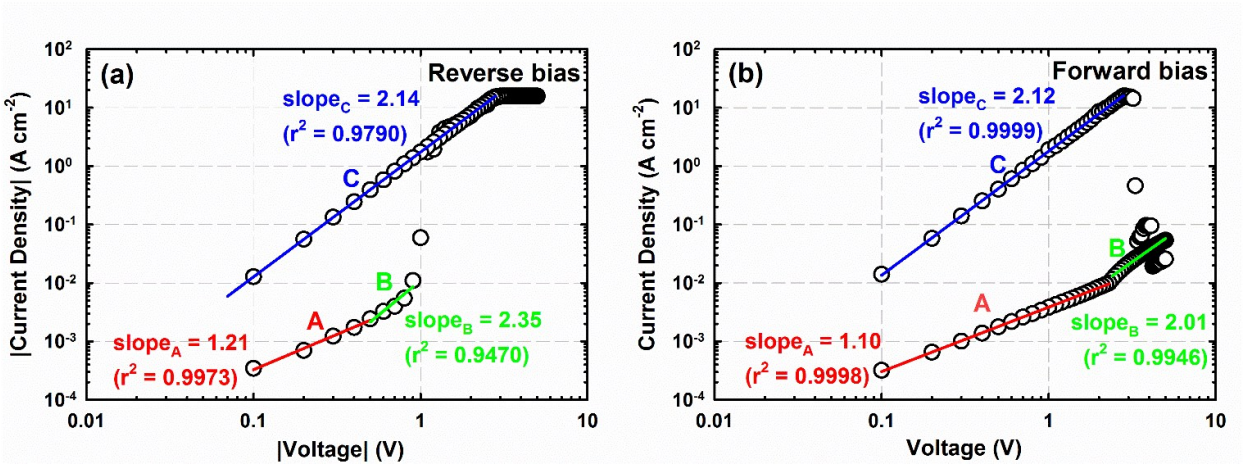

Figure 15. Full logarithmic *J-V* relationships of the Aloe vera-based memory device in (a) reverse bias and (b) forward bias region. Experimental data are represented by open symbols. Linear fitting to the experimental data are represented by solid lines.

chemical composition, especially the filament-forming species in the active layer. Electrochemical techniques such as cyclic voltammetry (CV) were used to determine the redox properties of the natural materials; whereas electrical techniques involve measuring the *J-V* characteristics using a Semiconductor Parameter Analyzer or a conductive atomic force microscopy (c-AFM). Among these techniques, electrical measurements represent one of the simple yet powerful technique for investigating not only filamentary conduction, but also other conduction mechanisms governing the memory device. Since most of the conduction mechanisms can be readily expressed by the relationships between *J* and *V*, by measuring the *J-V* curve of a memory device and plotting the data in a logarithmic scale, hence the conduction mechanism can be determined. In a typical filamentary conduction, *J* is in linear proportion to *V* (Ohm's law) in the ON-state due to the formation of filaments connecting both electrodes; whereas in the OFF-state, the current conduction is usually governed by a combination of Ohm's law and Child's law (as a whole it is termed as SCLC).[17,25]

To deduce the possible charge conduction mechanism in this work, the *J-V* curve of Aloe vera-based memory is measured and replotted into a log-log scale. Figure 15a shows the log *J* versus log *V* plot of the device in reverse bias region. Three distinct regions (region A, B, and C) indicate that conduction process in Aloe vera layer may be dominated by different conduction processes. In region A, the charge conduction process is obeying Ohm's law:[87,89]

$$J_{Ohm} = qn_0\mu\frac{V}{d} \quad (3)$$

where J_{Ohm}, q, n_0, μ, and d are the current density due to Ohmic conduction, electronic charge, charge density in thermal equilibrium, charge mobility, and thickness of the Aloe vera layer, respectively. Taking the logarithm on both sides of Equation 3, a linear *J-V* relationship with a unity slope can be easily observed. This is evidenced in Figure 15a where the linear fitting in region A yields a slope = 1.21, with a goodness of fit, r^2 = 0.9973. In region B, the current conduction in the Aloe vera-based device is governed by Child's law:[89]

$$J_{Child} = \frac{9}{8}\cdot\frac{n_0\varepsilon\mu}{N_t}\left(\frac{V^2}{d^3}\right) \quad (4)$$

where J_{Child}, ε, and N_t are the current density according to Child's law, electronic permittivity, and density of traps in the Aloe vera layer, respectively. Taking the logarithm on both sides of Equation 4, a linear *J-V* relationship with a slope = 2 can be evident. According to Equation 4, electrons injected from the top electrode are trapped in the Aloe vera layer, as indicated by the n_0/N_t ratio. Consequently, a space-charge region is formed at the Al/Aloe vera interface to impede further injection of electrons from the top electrode. The repulsion force of the space-charge region can only be overcome as the applied voltage is increased to a threshold trap-filled-limited (TFL) voltage:[89]

$$V_{TFL} = \frac{qN_t d}{2\varepsilon} \quad (5)$$

This V_{TFL} is also termed as V_{set} in the memory device based on Aloe vera. Beyond this critical voltage, an abrupt increase in current density can be observed and region C is achieved when charge traps in the Aloe vera layer are completely filled ($n_0 \approx N_t$) and Child's law (Equation 4) can be further simplified into

$$J_{TFL} = \frac{9}{8}\cdot\varepsilon\mu\left(\frac{V^2}{d^3}\right) \quad (6)$$

where J_{TFL} is the current due to TFL conduction. It is noteworthy that charge traps in this region are completely filled by injected charge carries, rather than absent from the Aloe vera layer. Similarly, TFL conduction governed by Child's law dominates the ON-state current conduction in the forward bias region (Figure 15b), while the OFF-state current conduction is controlled by a combination of Ohm's and Child's law, with the transition from ON to OFF-state occurs at the threshold TFL voltage (also termed as V_{reset} in memory device based on Aloe vera). In both forward and reverse bias *J-V*

characteristics, the current conduction in region A, B, and C is controlled by a combination of (i) Ohm's law, (ii) Child's law, and (iii) TFL conduction respectively. Since a combination of these three current limiting processes constitute the framework of SCLC,[87-89] a concluding remark can be made where the current conduction mechanism in Aloe vera-based memory device is dominated by the SCLC mechanism.

The conduction processes of the memory device based on Aloe vera can be explained schematically using band diagrams. The band diagram of the pristine memory device is depicted in Figure 16a. The work functions of top (Al) and bottom (ITO) electrodes are 4.1 and 4.7 eV respectively, in reference to the vacuum level (E_{vac}).[19] Generally, Charge carriers in a dried Aloe vera layer can either be acquired or generated either by (i) injection from the electrodes or (ii) thermal ionization within the material. The former process requires relatively high applied voltage if compared with the latter one. Due to sufficiently low voltage (0.0 to –0.5 V) applied to the top electrode at the early stage, thermally ionized electrons are generated within the Aloe vera layer, captured in trap centers, and then contributed to the relatively low level of current density (J_{ohm}) as illustrated in Figure 16b. Electrons are being injected into the Aloe vera layer as the voltage is increased. The presence of charge traps in the Aloe vera layer has caused the formation of space-charge region near to the Al/Aloe vera interface (Figure 16c). The electrical stress exerted by the space-charge region can only be overcome by applying a voltage larger than V_{TFL}. Beyond V_{TFL}, electrons captured by the charge traps are slowly escaping and transferring towards any unfilled charge traps with relatively lower energy level and are located at physically closer to the positively biased bottom electrode. Simultaneously, injection of electrons from top electrode (Process 1 in Figure 16d) is continuously supplying source of electrons to fill up the traps that have been emptied due to escape of electrons towards the bottom electrode (Process 2 in Figure 16d). Therefore, electrons are able to move from top electrode crossing the Aloe vera layer via randomly distributed trap centers and end up to the positively biased bottom electrode. The memory device is switched on, as indicated by a high level of current density.

As the negatively applied voltage to the top electrode is reducing from –5.0 V to 0 V, TFL conduction mechanism (Figure 16d) is still the dominant charge conduction for electrons to move from top to bottom electrode; maintaining the high level of current density and the device is still remain in ON-state. Both electron injection (Process 1 in Figure 16d) and extraction (Process 2 in Figure 16d) processes are reducing as the voltage is approaching 0 V, which is the flatband voltage of the system (Figure 16e). Even though the applied voltage is at 0 V, there are still some electrons that are immobilized and trapped in the Aloe vera layer with the device remains in its ON-state. The distribution of trapped electrons inside the Aloe vera layer is depending on the work functions of both top and bottom electrodes as shown schematically in Figure 16e. When a forward voltage sweeping from 0 to 3.1 V is applied, electrons are now being injected from bottom electrode (Process 1 in Figure 16f) and extracted at top electrode

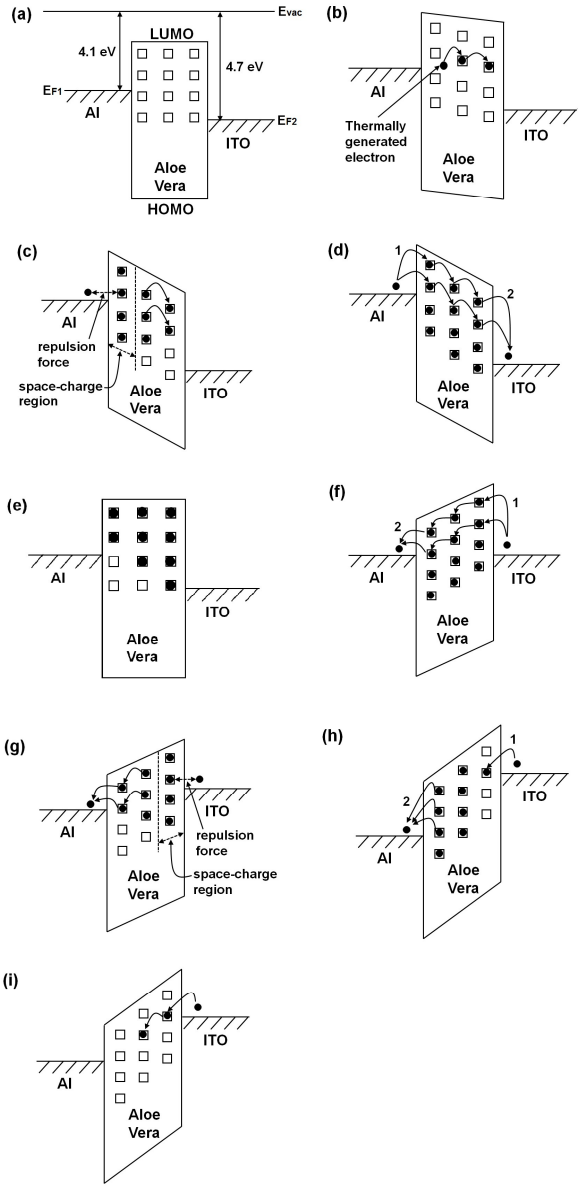

Figure 16. Schematic illustration of band diagram at different stages: (a) pristine test structure, (b) trap-filled-limited conduction, (c) build-up of space-charge region at top contact, (d) trap-free conduction during reverse bias sweep, (e) flatband voltage, (f) trap-free conduction during forward bias sweep, (g) build-up of space-charge at bottom contact, (h) ON-state conduction, and (i) trap-filled-limited conduction. Symbols "□" and "•" represent trap centers and electrons, respectively. Numbers 1 and 2 represent the electron injection and extraction processes, respectively.

(Process 2 in Figure 16f). Within this forward voltage sweeping range, equilibrium between injection and extraction rate of electron is achieved and hence charge conduction through the Aloe vera layer is observed with relatively high current density being recorded. This trap-free assisted conduction process is increasing as the forward bias voltage increases until 3.1 V.

When subjected to a forward bias voltage of 3.1 V, a relatively huge amount of electrons are being trapped and

located inside the Aloe vera and created a negative charge region. The built-in electric field in this region is repulsing the electrons, of the same polarity, trying to inject from the bottom electron into the Aloe vera layer. Therefore, a space-charge region is built up at the bottom electrode/Aloe vera interface (Figure 16g) preventing further injection of electrons to the Aloe vera. Hence, a drastic reduction in charge movement across the Aloe vera layer is observed and the current density is significantly reduced to a lower level and the device is now at its OFF-state. This particular voltage is termed as V_{reset} where the ON-state of the device is reset back it is original OFF-state.

As the forward bias at top electrode is further increasing from 3.1 V to 5.0 V, sufficiently high energy is gained by the trapped electrons in the Aloe vera layer and escaped towards the positively biased top electrode (Figure 16h). Those trapped electrons located physically closer to the top electrode/Aloe vera interface may have a higher probability to be escaped (Process 2 in Figure 16h) if compared with those located deeper in the Aloe vera. As the forward bias is increasing, electrons located at deeper traps are also able to be extracted and escaped. As a result, many unfilled traps are now available in the Aloe vera layer but the filling of the traps by the injection of electrons from the bottom electrode (Process 1 in Figure 16h) is relatively slow. With this process, TFL charge conduction has minimized the current flowing through the device and the OFF-state of the device is maintained until 5.0 V. As the reverse bias is applied to the top electrode from 5.0 V back to 0 V, injection of electrons from bottom electrode is continued Figure 16i). The injection is reducing as the applied voltage is approaching 0 V. The injected electrons are being trapped in Aloe vera but the probability of them to escape from the traps and end up to the top electrode is relatively low. Therefore, most of the injected electrons are being trapped in the Aloe vera and not contributing to any current flow. Hence, the memory device is remained in OFF-state until 0 V. It is noteworthy that the hysteresis of *J*–*V* plot is asymmetric due to the difference in the magnitudes of V_{set} and V_{reset}. V_{reset} occurs at a higher voltage of opposite polarity as compared with V_{set} owing to a higher work function of the bottom (ITO) electrode (4.7 eV) than the top (Al) electrode (4.1 eV).[19]

Physically, injected electrons are trapped in a center within the dried Aloe vera layer. These electron trap centers may be originated from the structural arrangement of polysaccharide chains in the Aloe vera gel. It has been reported that an electron in amorphous solids could be trapped in a small interstitial space formed by a few polar molecules and the state of trapped electron may be stabilized by both Coulomb attraction force and Pauli exclusion repulsive force exerted by the permanent dipoles of the molecules forming the interstitial space.[90,91] The proposed electron-trap center is illustrated in Figure 17. In general, this concept of electron-trap center may be viewed as a single quantum particle (the electron) in a three-dimensional potential well. The potential energy of the trap centers is dependent on the number of −OH groups forming the interstitial space.[90,91] The high amount of this group, the deeper trap can be formed in an interstitial space.[90,91] Based on the discussion and proposal outlined by TGA, when pure Aloe vera is heated above 50^{o}C, pectins may undergo de-esterification, while deacetylation of acemannan is promptly initiated. This results are further confirmed by the FTIR spectra where important reduction in peak intensity at 1743 and 1256 cm^{-1} due respectively to C=O and C−O−C stretching of $–COOCH_3$ and $–COCH_3$ groups of the carbohydrate polymers. These de-esterified pectin chains, together with the deacetylated acemannan chains, could interact with each other as proposed in Figure 17 to create clusters of trap centers.

In contrary, no memory-switching effect can be observed from the *J*–*V* characteristics of test structures with pure Aloe vera dried at 80°C and 120°C. The test structure dried at 80°C

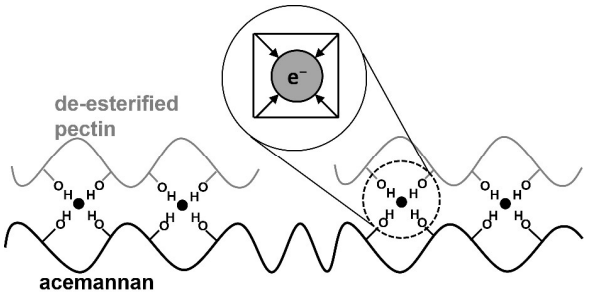

Figure 17. A proposed conceptual drawing of electron trap centers that may form by structural arrangement of acemannan and de-esterified pectin chains. The symbol "•" indicates an electron trapped at the center of an interstitial space. The arrow represents the positive end of the permanent dipole pointing to an electron.

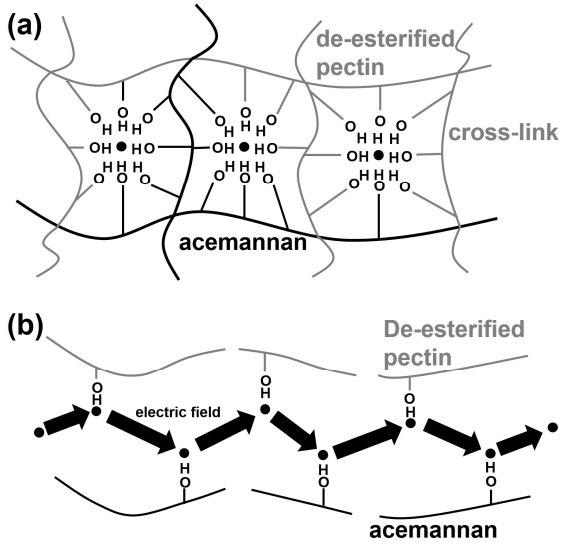

Figure 18. A proposed conceptual drawing of (a) cross-linked polysaccharide network of de-esterified pectins and acemannan and dried at 80°C that deep charge traps are formed and (b) structural defects as shallow charge traps in the Aloe vera layer as covalent bonds connecting the polysaccharide backbones are broken at 120°C. The symbol "•" indicates a trapped electron. The thick arrow in (b) represents the movement path of electrons towards direction of electric field.

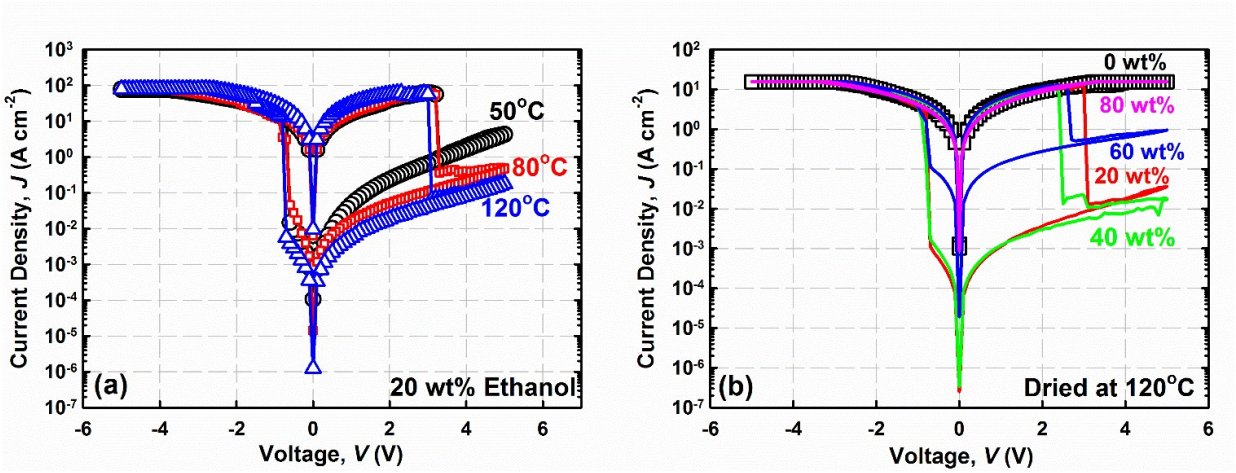

Figure 19. Representative family plots of J–V characteristics of test structures based on (a) Aloe vera added with 20 wt% of ethanol dried at 50°C, 80°C, and 120°C, and (b) Aloe vera added with different concentration (0, 20, 40, 60, and 80 wt%) of ethanol and dried at 120°C.

and 120°C record a low- and high-level of current density that is close to the OFF- and ON-state of memory characteristics recorded by pure Aloe vera dried at 50°C. The non-memory characteristics of the Aloe vera layers dried at temperature higher than 50°C can be elaborated as follows. At the drying temperature of 80°C, hydrolysis of pectin (Figure 11b) may create and contribute to additional uronic acids that can combine and interact with the de-esterified pectin and acemannan chains to form a cross-linked and branched polysaccharide network (Figure 18a). Due to higher amount of hydroxyl groups located at a specific interstitial space, the trap centers are now become deeper if compared to its counterpart dried at 50°C. When a voltage is applied, injected electrons are being captured in these deep traps. Consequently, a low leakage current density that conducted via TFL mechanism is recorded.

On the other hand, when the Aloe vera layer is dried at 120°C, pectin chains are degrading via β-elimination reactions (Figure 11c) and acemannan chains are dissociating due to thermal effect. The thermal energy is sufficiently high to break the covalently bonded backbone molecules of acemannan and pectin chains as well as to destroy any trap centers that being formed by –OH interaction. As a result, numerous structural defects are being formed at this relatively high temperature. The structural defect may act as a temporary and shallow electron trap center. When electrons are being injected from either bottom or top electrode, they are able to freely drift across the Aloe vera layer via trapping and de-trapping through these shallow as governed by the trap-free conduction mechanism (Figure 18b).

Figure 19a shows a representative family plot of *J*–*V* characteristics of test structures based on Aloe vera mixed with 20 wt% of ethanol and dried at different temperatures (50°C, 80°C, and 120°C). All of the test structures exhibit memory switching effect and can be utilized for memory application. If compared to the test structures based on pure Aloe vera, in which the memory switching effect can only be demonstrated at drying temperature of 50°C, test structures with 20 wt% of Aloe vera are able to demonstrate the memory switching effect at drying temperature as high as 120°C. Therefore, the drying temperature for which memory switching effect can be maintained is extended by mere addition of 20 wt% of ethanol to the Aloe vera gel. It has been reported that by adding appropriate amount of ethanol, cell wall tissues of fruits and vegetables can be preserved due to suppression of hydrolysis process (Figure 11b).[61-63] By limiting the hydrolysis, β-elimination in de-esterified pectin can be minimized and hence degradation of the de-esterified pectin chain can be prevented. With these, clusters of trap centers formed according to the proposed mechanism illustrated in Figure 17 are able to maintain even when the drying temperature is extended to 120°C.

Figure 19b shows a family plot of *J*–*V* characteristics of test structures with different concentration of ethanol added to Aloe vera and dried at a constant temperature of 120°C. Bipolar memory switching is clearly demonstrated by test structures with 20, 40, and 60 wt% of ethanol only. Test structures with 0 and 80 wt% of ethanol do not exhibit any memory switching effects. These two test structures have recorded a high-level of leakage current density that is similar to the level of ON-state of the other test structures showing memory-switching effect. Based on prior discussion, it is believed that the high leakage current density with non-memory switching effect may be explained by the mechanism proposed in Figure 18b. The dissociated, fragmented, and decomposed polysaccharides due to relatively high thermal budget to the Aloe vera may create structural defective and shallow trap centers, in which trap-free conduction mechanism is determining the transportation of electron through the dried Aloe vera layer.

Although the test structures with 20, 40, 60 wt% of ethanol exhibit memory switching effects, some variations in their *J*–*V* characteristics can be observed. One of the variations is the drastic reduction of OFF-state leakage current exhibited in the test structure with 60 wt% of ethanol. The reduction of OFF-state leakage current density is mainly due to the relatively

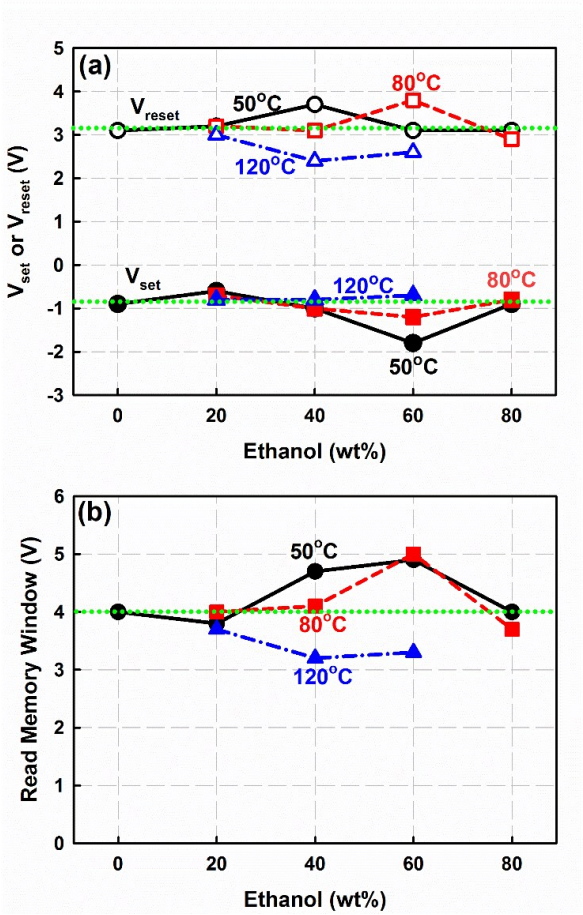

Figure 20. Plot of (a) V_{set} and V_{reset} and (b) read memory window as a function of ethanol concentration. The horizontal dotted lines refer to V_{set}, V_{reset}, and read memory window of test structure based on pure Aloe vera dried at 50°C.

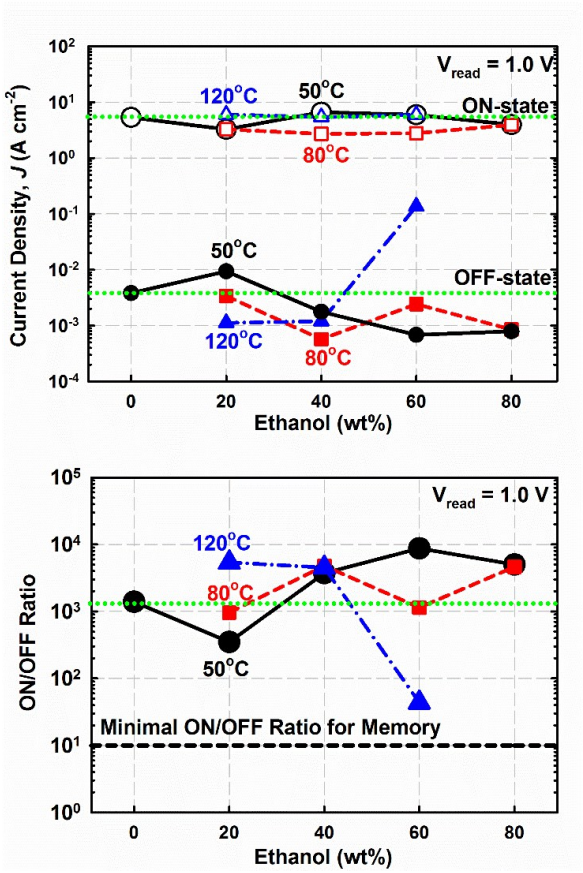

Figure 21. Plot of (a) current density in both OFF- and ON-state (b) ON/OFF ratio as a function of ethanol concentration. The horizontal dotted lines refer to the OFF- and ON-state current density as well as the ON/OFF ratio achieved by test structure based on pure Aloe vera dried at 50°C. The horizontal dash line refers to basic ON/OFF requirement proposed in Ref. 71.

lower degree of cross-linking of the Aloe vera layer. Cross-linking could lead to the formation of deep charge traps in the Aloe vera layer (Figure 18a). Thus, with a lower degree of cross-linking, a higher OFF-state leakage current is recorded in the test structure with 60 wt% of ethanol.

Figure 20a summarizes the values of V_{set} and V_{reset} extracted from the first SET/RESET cycle of test structures with Aloe vera having different concentration of ethanol and dried at different temperatures. The values of read memory window corresponding to these values (V_{set} and V_{reset}) are presented in Figure 20b. Since for the series of test structures based on pure Aloe vera (0 wt% of ethanol), the only test structure that demonstrates memory switching characteristics is the one dried at 50°C, it is used as a benchmark to gauge the effects of drying temperature and ethanol concentration on the read memory window. This particular test structure exhibits a V_{set} of −0.9 V and a V_{reset} of 3.1 V, which could be translated into a read memory window of 4.0 V. From Figure 20a, it can be noticed that distribution of V_{reset} values as a function of drying temperature and ethanol concentration falls within ±1.0 V of the V_{reset} value of test structure with pure Aloe vera. On the other hand, the values of V_{set} as a function of drying temperature and ethanol concentration appear to be rather consistent, despite a distribution of ±0.75 V against the V_{set} value recorded by test structure with pure Aloe vera. The distribution of V_{set} is mainly contributed by the series of test structure with 60 wt% of ethanol dried at different temperatures. Due to these variations, the resultant read memory window shows a distribution of about ±1.0 V against the benchmark test structure. The test structure of Aloe vera added with 80 wt% of ethanol and dried at 120°C demonstrates non-memory switching effect and the reason behind this observation have been explained in prior paragraph.

The read memory window of a memory device is closely associated with the V_{read} as shown in Figure 13. In general, the V_{read} is required to fall within the read memory window and it needs to be significantly smaller than the V_{set} and V_{reset} of the memory device to prevent a change of memory state during the read operation. Besides that, the selection of V_{read} is also subjected to the constraints imposed by the sensing circuits. For example, the ON-state current to be read by a sensing circuit should not be less than 1 μA to enable fast memory-state readout.[71] Therefore, a wide read memory window is

usually desirable when developing a memory device, to allow a greater degree of flexibility for which electronic application the memory device could be utilized.

Figure 21a summarizes the levels of current density in both OFF- and ON-state of all test structures at V_{read} = 1.0 V that have been extracted from the first SET/RESET cycle. The ON/OFF ratios corresponding to these current densities are presented in Figure 21b. The test structure based on pure Aloe vera is again used as the benchmark for comparing the current densities and ON/OFF ratios of other test structures as a function of drying temperature and ethanol concentration. The test structure with pure Aloe vera and dried at 50°C exhibits an ON-state current density of ~5.0×10^{0} A·cm^{-2} and an OFF-state current density of ~3.0×10^{-3} A·cm^{-2}, which yield an ON/OFF ratio of ~1.7×10^{3}. The levels of current density in the ON-state as a function of drying temperature and ethanol concentration appear to be relatively constant, despite with a distribution of less than ±1.0×10^{1} A·cm^{-2} against the benchmark. On the other hand, obvious variations in the OFF-state current densities with a distribution of about ±1.5×10^{1} A·cm^{-2} against the benchmark can be observed. The wider distribution of OFF-state current densities as compared to the ON-state is mainly attributed to the abrupt increment in OFF-state current of the test structure with Aloe vera having 60 wt% of ethanol and dried at 120°C. Because of these variations, the ON/OFF ratios of the test structures as a function of drying temperature and ethanol concentration shows a distribution of about ±1.5×10^{1} A·cm^{-2} against the benchmarking test structure based on pure Aloe vera.

The ON/OFF ratio represents an essential performance parameter of memory devices. It determines whether a memory state (ON- or OFF-state) could be distinguished by external sensing circuits. Although an ON/OFF ratio of ten is reasonably sufficient for advanced sensing circuits to differentiate a memory state,[71] memory device that could exhibit a large ON/OFF ratio is highly desirable and encouraged to avoid erroneous memory state readout.

A memory device is expected to store a bit of information for a prolonged period of time. A retention period of >10 years is generally required for all non-volatile memory technologies. In a typical retention test measurement, a pristine test structure with a low level of current density in its OFF-state was being used. The test structure is then switched to its ON-state by applying a reverse bias voltage of −1.5 V on the top

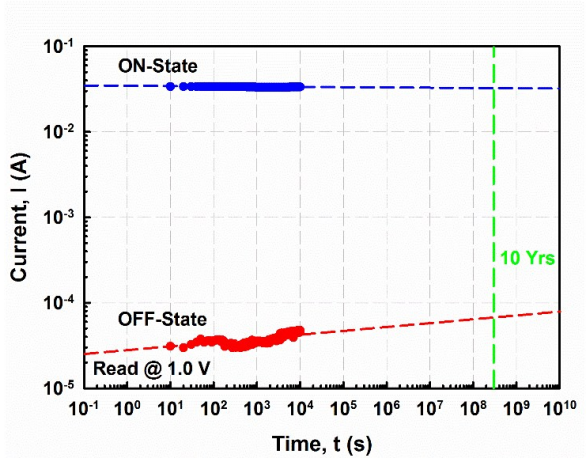

Figure 22. A representative retention characteristic of the test structure with 60 wt% of ethanol dried at 50°C. The ON- and OFF-state current was read (Vread) at 1.0 V.

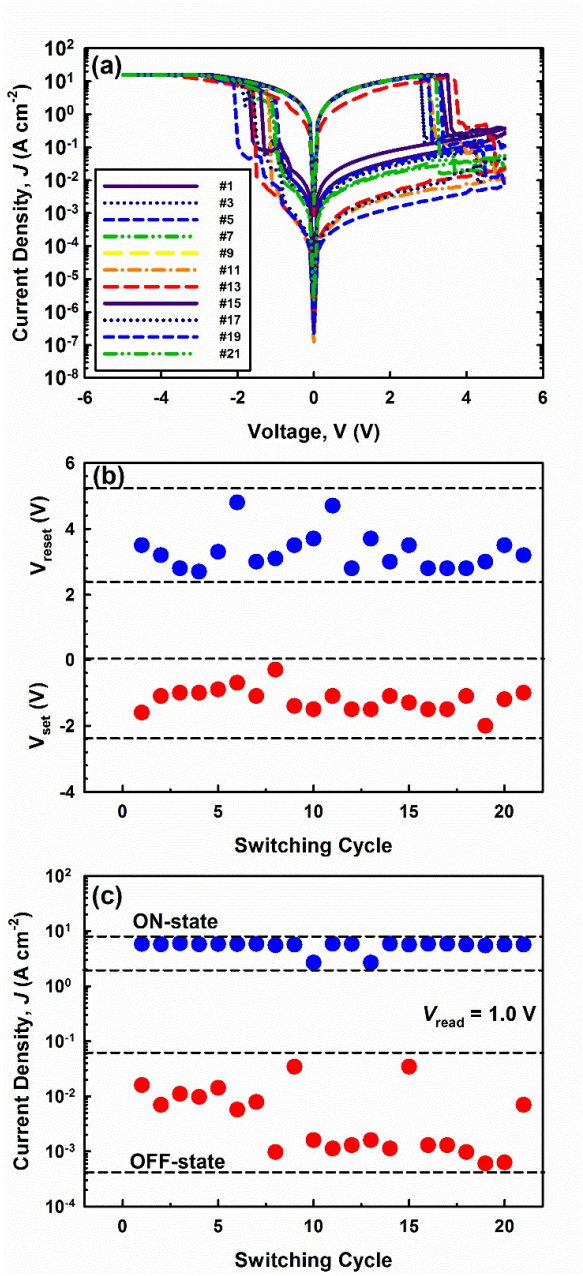

Figure 23. (a) A set of J–V characteristics revealing the endurance performance of the test structure with 60 wt% of ethanol dried at 50°C. (b) Distribution of Vset and Vreset values of the test structure over 21 switching cycles. (c) Distribution of OFF- and ON-state current densities of the test structure under a Vread of 1.0 V over 21 switching cycles.

Table 3. Summary of performance characteristics of memory devices based on various natural materials and selected polymers.

Natural material	Read memory window (V)	ON/OFF ratio	Retention time (s)	Endurance cycles	Ref.
Natural Aloe vera	5.0	10^3	$>10^4$	>21	This work
Tobacco mosaic virus	5.5	10^3	$>10^3$	>100	16
Ferritin	3.0	10^3	$>10^4$	>300	17
Lysozyme	2.3	10^3	$>10^4$	>200	18
Silk fibroin	15.5	10^1	$>10^3$	>120	19,20
Sericin	3.0	10^6	$>10^3$	>21	22
Silk fibroin-AuNPs	2.8	10^6	$>10^7$	>10	21
Cellulose nanofiber paper	0.5	10^7	$>10^5$	>100	23
Chitosan	1.0	10^5	$>10^4$	>100	24
DNA	1.6	10^2	$>10^6$	>100	25
Chicken egg albumen	3.6	10^3	$>10^4$	>500	26

electrode with the bottom electrode grounded the entire time. The ON-state current of the test structure is measured by applying a voltage pulse of 1.0 V at an interval of 10 s for 12 h. After that, the test structure is switched back to its OFF-state by applying a forward bias voltage of ~3.5 V. Measurement of the OFF-state current is repeated by applying a voltage pulse of 1.0 V at an interval of 10 s for 12 h. Figure 22 presents the representative retention characteristic of the test structure with 60 wt% of ethanol and dried at 50°C. The ON-state current remains relative constant at 3.0×10^{-2} A during the entire retention test measurement period and this stability should remain even when the data are projected to the 10-year horizon. On the other hand, the OFF-state current is not as stable as the ON-state current. Within a 12-hour retention test, the OFF-state current is increasing gradually from 2.4×10^{-5} to 5.0×10^{-5} A. The OFF-state is projected to rise to ~7.0×10^{-5} A at the end of 10-year horizon. In general, an ON/OFF ratio of ~10^3 can still be achieved after the test structure is extrapolated to 10 years.

In general, a test structure is expected to endure a finite number of SET/RESET cycles in order to be considered as a practical memory device. In a typical endurance test, the test structure was repeatedly switched between its OFF- and ON-state by applying appropriate voltage sweeps. To achieve this, a test structure was subjected to voltage of the sequence: 0 → −5 V, −5 → 0 V, 0 → 5, and 5 → 0 V. Figure 23a shows the *J*–*V* characteristics of the test structure with 60 wt% of ethanol, dried at 50°C, and tested repeatedly for over 21 SET/RESET cycles. The test structure demonstrates consistent memory switching between its OFF- and ON-state throughout the cycles, despite some variations in the threshold voltages (V_{set} and V_{reset}) and current density in both OFF- and ON-state. Figure 23b shows the distribution of V_{set} and V_{reset} extracted from the *J*-*V* characteristics of the test structure over 21 cycles. The minimum difference between the V_{set} and V_{reset} values is approximately 2.4 V, while the average values for V_{set} and V_{reset} are −1.2 V and 3.1 V, respectively. The values of V_{set} distributes over the range of ±1.2 V against the average V_{set} values, while the distribution of V_{reset} values spans over the range of ±2.1 V. These distribution trends are in agreement with the distribution of V_{set} and V_{reset} against the test structure based on pure Aloe vera shown in Figure 20a. The values of V_{reset} distribute over a wider range than the values of V_{set}. Figure 23c shows the distribution of current densities in both OFF- and ON-state of the test structure over 21 cycles. The current densities are extracted using a read voltage of 1.0 V. The minimum difference between the OFF- and ON-state current densities is 3.3×10^1 A·cm^{-2}. It can be observed that the values of OFF-state current density distributes over the range of ±1.5 $\times 10^1$ A·cm^{-2} against the average value of 7.6×10^{-3} A·cm^{-2}, while the values of ON-state current density distribute over range of less than ±1.0×10^0 A·cm^{-2} against the average value of 5.5×10^0 A·cm^{-2}. Similar to the distribution of V_{set} and V_{reset} values, the distribution trends of both OFF- and ON-state current densities are in agreement with the distribution against the test structure based on pure Aloe vera (Figure 21b). The OFF-state current density fluctuates over a wider range if compared to the values of ON-state current density. Nevertheless, the endurance properties of the device can be considered reasonable with no significant deterioration detected.

Besides natural Aloe vera, several natural materials have been used to develop memory devices. Table 3 summarizes the memory devices based on natural materials and their performance parameters. In comparison, the natural Aloe vera-based memory device achieves reasonably good performance, with a relatively wide read memory window (~5.00 V), large ON/OFF ratio (>10^3), and good retention performance (>10^4 s).

Conclusions

In this work, it has been proven that extraction of natural Aloe vera after processing with different concentrations of ethanol (0, 20, 40, 60, and 80 wt%), spin-coated on an ITO glass substrate, and dried at different temperatures (50, 80, and 120°C) could demonstrate bipolar memory-switching effects. The functional memory device realized in a metal-Aloe vera-metal structure with Al and ITO as the top and bottom electrodes has been fabricated. Current density-voltage characteristic measurement on the test structures has been performed before the thermal, structural and functional group of the processed Aloe vera have been investigated. For a memory device with pure Aloe vera and dried at 50°C, a read memory window of ~4.0 V and an ON/OFF ratio of ~10^3 (read

at 1.0 V) have been recorded. The reproducible memory switching between low current density OFF-state and high current density ON-state is governed by SCLC. The origin of the charge trap centers is elucidated as the structural arrangement of pectins and acemannans in the pure Aloe vera layer. In this context, the terminal functional groups of the polysaccharides could arrange such that an interstitial space which could act as a three dimensional potential well with electron trapping capability. In contrary, pure Aloe vera dried at 80°C and 120°C in a similar test structure do not show any memory switching effects. However, by addition of appropriate amount of ethanol, the range of drying temperature could be extended. It has been demonstrated that by adding 20, 40, and 60 wt% of ethanol, the drying temperature of Aloe vera layer could be extended to 120°C except for the layer with 80 wt% of ethanol that only revealed the memory effect when dried until 80°C. It is proposed that by adding ethanol in Aloe vera, hydrolysis and β-elimination reaction of pectins could be slow down. With the preservation of pectins, formation of cross-linked and branched polysaccharide network with large amounts of deep charge traps could be prevented. It has been demonstrated that memory devices based on Aloe vera with 60 wt% of ethanol dried at 50°C could endure for 21 cycles of SET/RESET operations. The retention test reveals that this memory device could retain data in its respective OFF- and ON-state for a period of about 12 h and it still remains stable when the retention test is mathematically extrapolated to a longer period of 10 years. Application of natural materials in electronic fabrication represents not only a compelling concept but it could also help in overcome e-waste crisis that may come along with the rapid progress in electronics industry. It is anticipated that more natural materials could be used in a wide array of electronic applications.

Acknowledgements

This work was supported by Fundamental Research Grant Scheme (FRGS, 203/PBAHAN/6071301), Research University-Individual Grant (RUI, 1001/PBAHAN/814216), and USM Postgraduate Research Grant Scheme (PRGS, 1001/PBAHAN/8036018). Z. X. Lim acknowledges the MyBrain15–MyPhD scholarship given by Ministry of Higher Education Malaysia.

References

1 J. Gubbi, R. Buyya, S. Marusic and M. Palaniswami, *Future Gener. Comp. Sy.*, 2013, **29**, 1645-1660.
2 S. Bauer and M. Kaltenbrunner, *ACS Nano*, 2014, **8**, 5380-5382.
3 R. W. Lucky, *IEEE Spectr.*, 2012, **49**, 34.
4 S. Mühl and B. Beyer, *Electronics*, 2014, **3**, 444.
5 J. Kuczynski and D. J. Boday, *Int. J. Sust. Dev. World*, 2012, **19**, 557-563.
6 N. Savage, *IEEE Spectr.*, 2015, **52**, 18.
7 M. Irimia-Vladu, E. D. Głowacki, G. Voss, S. Bauer and N. S. Sariciftci, *Mater. Today*, 2012, **15**, 340-346.
8 M. Irimia-Vladu, N. S. Sariciftci and S. Bauer, *J. Mater. Chem.*, 2011, **21**, 1350-1361.
9 M. Irimia-Vladu, *Chem. Soc. Rev.*, 2014, **43**, 588-610.
10 Y. H. Jung, T.-H. Chang, H. Zhang, C. Yao, Q. Zheng, V. W. Yang, H. Mi, M. Kim, S. J. Cho, D.-W. Park, H. Jiang, J. Lee, Y. Qiu, W. Zhou, Z. Cai, S. Gong and Z. Ma, *Nat. Commun.*, 2015, **6**.
11 J.-W. Chang, C.-G. Wang, C.-Y. Huang, T.-D. Tsai, T.-F. Guo and T.-C. Wen, *Adv. Mater.*, 2011, **23**, 4077-4081.
12 J. A. Hagen, W. Li, A. J. Steckl and J. G. Grote, *Appl. Phys. Lett.*, 2006, **88**, 171109.
13 Irimia-Vladu, P. A. Troshin, M. Reisinger, G. Schwabegger, M. Ullah, R. Schwoediauer, A. Mumyatov, M. Bodea, J. W. Fergus, V. F. Razumov, H. Sitter, S. Bauer and N. S. Sariciftci, *Org. Electron.*, 2010, **11**, 1974-1990.
14 M. Irimia-Vladu, P. A. Troshin, M. Reisinger, L. Shmygleva, Y. Kanbur, G. Schwabegger, M. Bodea, R. Schwödiauer, A. Mumyatov, J. W. Fergus, V. F. Razumov, H. Sitter, N. S. Sariciftci and S. Bauer, *Adv. Funct. Mater.*, 2010, **20**, 4069-4076.
15 Q.-D. Ling, D.-J. Liaw, C. Zhu, D. S.-H. Chan, E.-T. Kang and K.-G. Neoh, *Prog. Polym. Sci.*, 2008, **33**, 917-978.
16 R. J. Tseng, C. Tsai, L. Ma, J. Ouyang, C. S. Ozkan and Y. Yang, *Nat. Nanotechnol.*, 2006, **1**, 72-77.
17 Y. Ko, Y. Kim, H. Baek and J. Cho, *ACS Nano*, 2011, **5**, 9918-9926.
18 H. Baek, C. Lee, K.-i. Lim and J. Cho, *Nanotechnology*, 2012, **23**, 155604.
19 M. K. Hota, M. K. Bera, B. Kundu, S. C. Kundu and C. K. Maiti, *Adv. Funct. Mater.*, 2012, **22**, 4493-4499.
20 C. Mukherjee, M. K. Hota, D. Naskar, S. C. Kundu and C. K. Maiti, *Phys. Status Solidi A*, 2013, **210**, 1797-1805.
21 N. Gogurla, S. P. Mondal, A. K. Sinha, A. K. Katiyar, W. Banerjee, S. C. Kundu and S. K. Ray, *Nanotechnology*, 2013, **24**, 345202.
22 H. Wang, F. Meng, Y. Cai, L. Zheng, Y. Li, Y. Liu, Y. Jiang, X. Wang and X. Chen, *Adv. Mater.*, 2013, **25**, 5498-5503.
23 K. Nagashima, H. Koga, U. Celano, F. Zhuge, M. Kanai, S. Rahong, G. Meng, Y. He, J. De Boeck, M. Jurczak, W. Vandervorst, T. Kitaoka, M. Nogi and T. Yanagida, *Sci. Rep.*, 2014, **4**.
24 N. Raeis Hosseini and J.-S. Lee, *ACS Nano*, 2015, **9**, 419-426.
25 S. Qin, R. Dong, X. Yan and Q. Du, *Org. Electron.*, 2015, **22**, 147-153.
26 Y.-C. Chen, H.-C. Yu, C.-Y. Huang, W.-L. Chung, S.-L. Wu and Y.-K. Su, *Sci. Rep.*, 2015, **5**.
27 T. Reynolds and A. C. Dweck, *J. Ethnopharmacol.*, 1999, **68**, 3-37.
28 K. Eshun and Q. He, *Crit. Rev. Food Sci. Nutr.*, 2004, **44**, 91-96.
29 J. Hamman, *Molecules*, 2008, **13**, 1599.
30 E. R. Rodríguez, J. D. Martín and C. D. Romero, *Crit. Rev. Food Sci. Nutr.*, 2010, **50**, 305-326.
31 A. G. Volkov, R. D. Lang and M. I. Volkova-Gugeshashvili, *Bioelectrochemistry*, 2007, **71**, 192-197.
32 A. G. Volkov, K. Baker, J. C. Foster, J. Clemmons, E. Jovanov and V. S. Markin, *Bioelectrochemistry*, 2011, **81**, 39-45.
33 A. G. Volkov, J. C. Foster, E. Jovanov and V. S. Markin, *Bioelectrochemistry*, 2011, **81**, 4-9.
34 L. Q. Khor and K. Y. Cheong, *J Mater Sci: Mater Electron*, 2013, **24**, 2646-2652.
35 L. Q. Khor and K. Y. Cheong, *ECS J. Solid State Sci. Technol.*, 2013, **2**, P440-P444.
36 R. Al Amin, S. M. Rana, S. H. Talukder, M. S. Iqbal, M. Anzan-Uz-Zaman and M. Hoq, *J. Appl. Sci.*, 2014, **14**, 3507.
37 A. G. Volkov, J. Reedus, C. M. Mitchell, C. Tucket, V. Forde-Tuckett, M. I. Volkova, V. S. Markin and L. Chua, *Plant Signal Behav.*, 2014, **9**, e29056.
38 K. Y. Cheong, S. Sreenivasan, K. A. Razak, Z. X. Lim, P. L. Tan and L. Q. Khor, presented in part at the The 8th International

Conference on Advanced Materials Processing, Hotel Grand Chancellor Sufers Paradise, Gold Coast, Australia, July 27-30, 2014, 2014.
39 W. F. Lim, H. J. Quah, S. Sreenivasan and K. Y. Cheong, *Mater. Technol.*, 2015, **30**, A29-A35.
40 T. A. P. Group, *Bot. J. Linn. Soc.*, 2009, **161**, 105-121.
41 A. Femenia, E. S. Sánchez, S. Simal and C. Rosselló, *Carbohydr. Polym.*, 1999, **39**, 109-117.
42 A. Femenia, P. García-Pascual, S. Simal and C. Rosselló, *Carbohydr. Polym.*, 2003, **51**, 397-405.
43 Y. Ni, D. Turner, K. M. Yates and I. Tizard, *Int. Immunopharmacol.*, 2004, **4**, 1745-1755.
44 M. D. Boudreau and F. A. Beland, *J. Environ. Sci. Heal. C*, 2006, **24**, 103-154.
45 V. M. Rodríguez-González, A. Femenia, R. F. González-Laredo, N. E. Rocha-Guzmán, J. A. Gallegos-Infante, M. G. Candelas-Cadillo, P. Ramírez-Baca, S. Simal and C. Rosselló, *Carbohydr. Polym.*, 2011, **86**, 1675-1683.
46 J. T.-N. Chow, D. A. Williamson, K. M. Yates and W. J. Goux, *Carbohydr. Res.*, 2005, **340**, 1131-1142.
47 J. J. Barlow, A. P. Mathias, R. Williamson and D. B. Gammack, *Biochem. Biophys. Res. Commun.*, 1963, **13**, 61-66.
48 G. A. Jeffrey and W. Saenger, *Hydrogen bonding in biological structures*, Springer, Berlin, 2012.
49 J. J. Moré, in *Numerical analysis*, Springer, 1978, pp. 105-116.
50 F. Nejatzadeh-Barandozi and S. T. Enferadi, *Org. Med. Chem. Lett.*, 2012, **2**, 1-9.
51 P. Jithendra, A. M. Rajam, T. Kalaivani, A. B. Mandal and C. Rose, *ACS Appl. Mater. Inter.*, 2013, **5**, 7291-7298.
52 A. Ray and S. M. Aswatha, *Ind. Crop. Prod.*, 2013, **48**, 36-42.
53 N. R. Swami Hulle, K. Patruni and P. S. Rao, *J. Food Process Eng.*, 2014, **37**, 375-386.
54 A. R. Fajardo, L. C. Lopes, A. G. B. Pereira, A. F. Rubira and E. C. Muniz, *Carbohydr. Polym.*, 2012, **87**, 1950-1955.
55 R. Gentilini, S. Bozzini, F. Munarin, P. Petrini, L. Visai and M. C. Tanzi, *J. Appl. Polym. Sci.*, 2014, **131**, 39760-39769.
56 A. R. Eberendu, G. Luta, J. A. Edwards, B. H. McAnalley, B. Davis, S. Rodriguez and C. Ray Henry, *J. AOAC Int.*, 2005, **88**, 684-691.
57 J. Simões, F. M. Nunes, P. Domingues, M. A. Coimbra and M. R. Domingues, *Carbohydr. Polym.*, 2012, **90**, 229-236.
58 I. C. Dea, A. H. Clark and B. V. McCleary, *Carbohydr. Res.*, 1986, **147**, 275-294.
59 A. Fellah, P. Anjukandi, M. R. Waterland and M. A. K. Williams, *Carbohydr. Polym.*, 2009, **78**, 847-853.
60 O. Kurita, T. Fujiwara and E. Yamazaki, *Carbohydr. Polym.*, 2008, **74**, 725-730.
61 R. L. Jackman, H. J. Gibson and D. W. Stanley, *Physiol. Plant.*, 1992, **86**, 600-608.
62 M. Knee, *Phytochemistry*, 1973, **12**, 1543-1549.
63 H. F. Linskens and J. F. Jackson, *Plant cell wall analysis*, Springer, Berlin, 2012.
64 P. Massiot, V. Perron, A. Baron and J. F. Drilleau, *LWT Food Sci. Technol.*, 1997, **30**, 697-702.
65 N. R. Swami Hulle, N. Kaushik and P. S. Rao, *Int. J. Food Prop.*, 2014, **18**, 1597-1612.
66 N. R. Swami Hulle and P. S. Rao, *Drying Technol.*, 2015, DOI: 10.1080/07373937.2015.1037887, null-null.
67 X. L. Chang, C. Wang, Y. Feng and Z. Liu, *J. Food Eng.*, 2006, **75**, 245-251.
68 J. M. Valverde, D. Valero, D. Martínez-Romero, F. Guillén, S. Castillo and M. Serrano, *J. Agric. Food Chem.*, 2005, **53**, 7807-7813.
69 S. Benítez, I. Achaerandio, F. Sepulcre and M. Pujolà, *Postharvest Biol. Tec.*, 2013, **81**, 29-36.
70 D. Rodrigo, C. Cortés, E. Clynen, L. Schoofs, A. V. Loey and M. Hendrickx, *Food Res. Int.*, 2006, **39**, 440-448.
71 R. Waser, R. Dittmann, G. Staikov and K. Szot, *Adv. Mater.*, 2009, **21**, 2632-2663.
72 B. L. Yang, P. T. Lai and H. Wong, *Microelectron. Reliab.*, 2004, **44**, 709-718.
73 P. K. Abraham and K. Sathianandan, *Thin Solid Films*, 1988, **164**, 353-356.
74 A. Prakash, J. Ouyang, J.-L. Lin and Y. Yang, *J. Appl. Phys.*, 2006, **100**, 054309.
75 J. Ouyang, C.-W. Chu, C. R. Szmanda, L. Ma and Y. Yang, *Nat. Mater.*, 2004, **3**, 918-922.
76 M. A. Reed, J. Chen, A. M. Rawlett, D. W. Price and J. M. Tour, *Appl. Phys. Lett.*, 2001, **78**, 3735-3737.
77 B. Cho, J.-M. Yun, S. Song, Y. Ji, D.-Y. Kim and T. Lee, *Adv. Funct. Mater.*, 2011, **21**, 3976-3981.
78 S. Wu, T. Tsuruoka, K. Terabe, T. Hasegawa, J. P. Hill, K. Ariga and M. Aono, *Adv. Funct. Mater.*, 2011, **21**, 93-99.
79 F. Pan, S. Gao, C. Chen, C. Song and F. Zeng, *Mater. Sci. Eng. R-Rep.*, 2014, **83**, 1-59.
80 J. H. A. Smits, S. C. J. Meskers, R. A. J. Janssen, A. W. Marsman and D. M. de Leeuw, *Adv. Mater.*, 2005, **17**, 1169-1173.
81 F. Verbakel, S. C. J. Meskers and R. A. J. Janssen, *Chem. Mater.*, 2006, **18**, 2707-2712.
82 A. Bandyopadhyay and A. J. Pal, *Appl. Phys. Lett.*, 2004, **84**, 999-1001.
83 B. Mukherjee and A. J. Pal, *Synt. Met.*, 2005, **155**, 336-339.
84 S. L. Lim, Ling, E. Y. H. Teo, C. X. Zhu, D. S. H. Chan, E.-T. Kang and K. G. Neoh, *Chem. Mater.*, 2007, **19**, 5148-5157.
85 A. Beck, J. G. Bednorz, C. Gerber, C. Rossel and D. Widmer, *Appl. Phys. Lett.*, 2000, **77**, 139-141.
86 A. Odagawa, H. Sato, I. H. Inoue, H. Akoh, M. Kawasaki, Y. Tokura, T. Kanno and H. Adachi, *Phys. Rev. B*, 2004, **70**, 224403.
87 K. Y. Cheong, J. H. Moon, H. J. Kim, W. Bahng and N.-K. Kim, *J. Appl. Phys.*, 2008, **103**, 084113.
88 H.-T. Lin, Z. Pei and Y.-J. Chan, *IEEE Electron Device Letters*, 2007, **28**, 569-571.
89 D. M. Taylor, *IEEE Trans. Dielectr. Electr. Insul*, 2006, **13**, 1063-1073.
90 I. A. Shkrob and M. C. Sauer, *J. Phys. Chem. A*, 2006, **110**, 8126-8136.
91 I. A. Shkrob and J. A. Schlueter, *Chem. Phys. Lett.*, 2006, **431**, 364-369.